January 2016

A micromechanical fracture model for ductile-brittle interfaces

Dhrubajyoti Datta
Purdue University

Graduate School Form
30 Updated 12/26/2015

PURDUE UNIVERSITY
GRADUATE SCHOOL
Thesis/Dissertation Acceptance

This is to certify that the thesis/dissertation prepared

By DHRUBAJYOTI DATTA

Entitled
A MICROMECHANICAL FRACTURE MODEL FOR DUCTILE-BRITTLE INTERFACES

For the degree of Master of Science in Civil Engineering

Is approved by the final examining committee:

AMIT VARMA
Co-chair

VIKAS TOMAR
Co-chair

AYHAN IRFANOGLU

To the best of my knowledge and as understood by the student in the Thesis/Dissertation Agreement, Publication Delay, and Certification Disclaimer (Graduate School Form 32), this thesis/dissertation adheres to the provisions of Purdue University's "Policy of Integrity in Research" and the use of copyright material.

Approved by Major Professor(s): AMIT VARMA, VIKAS TOMAR

Approved by: DULCY ABRAHAM 04/14/2016

Head of the Departmental Graduate Program Date

A MICROMECHANICAL FRACTURE MODEL FOR DUCTILE-BRITTLE INTERFACES

A Thesis

Submitted to the Faculty

of

Purdue University

by

Dhrubajyoti Datta

In Partial Fulfillment of the

Requirements for the Degree

of

Master of Science in Civil Engineering

May 2016

Purdue University

West Lafayette, Indiana

For Ma and Baba

ACKNOWLEDGEMENTS

I am highly grateful and indebted to my advisors, Dr. Amit Varma and Dr. Vikas Tomar, whose understanding, expertise and generous guidance made it possible for me to pursue this interdisciplinary topic which was of great interest to me.

I would also like to thank Dr. Ayhan Irfanoglu for serving on the examining committee and providing constructive critiquing, comments and suggestions.

I express my deepest gratitude to all my professors, whose inputs have allowed me to develop the fundamental concepts which were quintessential to refine my research.

I would like to thank the administrative staff at Structures area of Lyles School of Civil Engineering department for helping with the formatting requirements and other formalities.

Lastly, I would express my sincere gratitude to my colleagues at Bowen Laboratory and Interfacial Multiphysics Laboratory for providing useful inputs.

TABLE OF CONTENTS

Page

LIST OF TABLES

Table Page

LIST OF FIGURES

Figure Page

Figure Page

LIST OF ABBREVIATIONS

SC: Steel Concrete

CTOD: Crack Tip Opening Displacement

SERR: Strain Energy Release Rate

SIF: Stress Intensity Factor

VCCT: Variable Crack Closure Technique

pz: process zone

XFEM: eXtended Finite Element Method

MAXPS: Maximum Principal Stress

SSI: Soil Structure Interaction

ABSTRACT

Datta, Dhrubajyoti. M.S.C.E., Purdue University, May 2016. Micromechanical fracture model of ductile-brittle bimaterial interface. Major Professors: Dr. Amit H. Varma and Dr. Vikas Tomar.

The micromechanical properties of a bimaterial interface depend on the (i) bonded slip and friction parameters (ii) release of fracture energy during crack growth and (iii) propagation, residual energy and shape formulations defining the failure envelope. A non-empirical fracture model is proposed for a ductile-brittle bimaterial interface. Such interfaces occur in Steel-Concrete (SC) composite wall modules, which are building blocks of nuclear and containment facilities. Similar bimaterial interfaces can occur in geotechnical structures, aerospace, ceramics and other composite applications. The thesis identifies the primary microstructural failure modes associated with such interfaces. A controlled volume fracture model for adhesively bonded interfaces is used in conjunction with Rice's [1] path independent J-Integral to correlate the strain energy release rate(SERR) to traction slip parameters. The linear elastic fracture model is modified to account for plasticity effects in the process zone and derive the crack tip opening displacement (CTOD). Numerical evaluation of fracture toughness parameters is performed to study impinging effects and determination of stress intensity factors. Depending on the nature of interface under consideration; appropriate tension

softening/hardening laws are incorporated to capture the phase transformation of crack propagation in the expression of J for remote integral paths,.

CHAPTER 1. INTRODUCTION AND BACKGROUND

Interfaces have always played a crucial role in material design, structural behavior, and biological transport phenomenon. The junction between two surfaces is not just an assumptive parameter but exhibits properties characteristic to both materials, and helps in facilitating transfer of stresses or tractions.

Ductile-brittle interfaces are an intrinsic part of aviation composite laminates, structural steel-concrete composites, ceramics, retrofits, and soil-structure interaction problems. In the field of composites, delamination is possibly the most critically studied failure mode, generally presumed to occur at the interface between adjoining plies and regarded as a fracture phenomenon between anisotropic layers. The Virtual Crack Closure Technique [2] was established on Irwin's argument that if a crack undergoes extension, the energy absorbed during the process is equivalent to the work done to close the crack to its initial configuration. It was developed to understand the strain energy release rate, interlaminar tension and scissoring shear stresses at discontinuities that result in mixed-mode delamination. As far as non-linearity and directionality is concerned; VCCT's application is limited to thin layered plane stress problems, since only cracks with single tip openings can be propagated. Presence of oscillating singularities at crack

tip makes it difficult to assess the energy release into the process zone. The tensile fracture behavior of mechanically nanostructured unreinforced alloys (Al-Al_2O_3 being the most popular) and fuselage-stringer welds are of prime importance to the aerospace industry. Insufficient bonding conditions pertaining to time, temperature and pressure lead to void formation, precipitation of undesired phases or undesired growth of fused grains resulting in interfacial cracks [3]. Experimental investigation suggests failure of Al_2O_3-metal interface occurs due to plastic deformation of metal matrix and elastic separation of alumina particulates with degradation of tensile ductility suggesting strain softening. Separation occurs at matrix process zone rather than reinforcing alumina. Most bimaterial energy-based fracture models fall short of defining the crack initiation criterion and accounting for plasticity effects of such interfaces. Recent studies indicate that interfaces play a key role in addressing durability requirements for ceramics and bi-layered structural materials subjected to progressive corrosion and moisture effects. Humid environment can have detrimental effects on reinforced concrete elements wrapped with FRP sheets after prolonged exposure. Cracks can either propagate in bulk media (material decohesion) or along the interface (material separation)[4]. In coastal areas corrosion of concrete due to chloride ingress or sulfate attack is a common thermo-chemical phenomenon; which can be explained as a pseudo-static process allowing crack fronts to initiate through internal microscopic volume expansion.

The fundamental marker for interfacial fracture of bimaterials is the fracture energy associated with it; and is responsible for influencing micromechanical properties (stress intensity factors and fracture toughness parameters) of composites, the damage of

bonds and delamination of thin films. The strain energy usually exceeds the thermodynamic work of adhesion due to mode mixity (shearing and opening) and presence of segregants at the interface; shielding caused by roughness and plasticity at crack tip [5]. The primary aim of interfacial fracture mechanics is to define the toughness parameter which characterizes fracture resistance. Solutions to such plane problems of interfacial cracks in heterogeneous media were presented half a century ago. On considering dissimilar materials with semi-infinite cracks, it was observed that stresses possess an oscillating singularity at crack tip [6], and this was further expanded to the case of flexural loading [7]. The eigen-function expansion approach adopted failed to quantitatively characterize stresses in the immediate vicinity of the crack tip [6], and was later integrated with complex potential functions to provide satisfactory evaluation of stress intensity factors [8]. The complex stress intensity factor ignored contact and was valid only for small scale non-linear behavior or negligible contact zone at the crack tip, which requires alteration of magnitude and phase angle of combined shear or tensile loading [9].

The present work focuses on developing models that can surpass difficulties [6, 7, 15, 19] associated with singularities at crack tip using fundamental energy conservation principles without delving into complex mathematical formulations. The model presented treats the interface crack as a boundary value problem; and is capable of computing strain energy release rates and crack tip opening displacements from specified far field stresses and tractions using path independent contour integrals.

In view of efforts to develop high performance concrete (a brittle bimaterial composed of mortar and matrix), deformations of mortar-matrix interface are

characterized based on fracture toughness parameters and transfer of stresses between phases of concrete. The load transfer is controlled by degree of contact and cohesive forces, which is improved upon thickness reduction of the interface [10]. The fracture toughness for a dissimilar brittle interface is assessed; considering plane strain deformation of a semi-infinite crack located along the interface between two isotropically homogeneous domains, by adopting *Dundur's(1969)*[11] moduli mismatch parameters, to derive a complex representation of the normal and shear stress fields in the vicinity of crack tip in terms of the interface stress intensity factor. Failure patterns have revealed that fracture propagation/kinking is often influenced by the phase angle and duration of loading, and have been verified by Brazilian Disc tests [12]. However, for ductile-quasi brittle interfaces (e.g. steel-concrete) bond cracks do not form in conjunction with mortar cracks, and there is a time lag between their propagation. The damage model presented in the study associates the lag to plasticity effects and slipping or pullout failure are the governing failure modes instead of transgranular cracking or aggregate interlock followed by debonding.

In order to comprehend the concealed mechanisms and structure of interfaces along with their mechanical strength, proper experimentation techniques are needed. One of the most popular stable fracture mechanics tests for bimaterial interfaces is the wedge splitting test[13] which is capable of determining fracture energy(G_F) and strain softening through a deformation-controlled uniaxial test. The primary focus is to measure the fracture energy required to split the specimen into two halves which is denoted by the area under the F_s vs. CTOD curve, spread over the projected area. A quasi-static mixed-

mode fracture criterion is obtained by plotting interlaminar fracture toughness against mode mix ratio, obtained from data generated using pure mode I Double Cantilever Beam tests, pure mode II End Notched Flexure tests, and Mixed Mode Bending tests of varying ratios. But, the fracture criterion is determined on the basis of curve fitting techniques, as the total energy release rate surpasses the toughness ratio. The wedge splitting test was further modified to determine the stress-crack opening relationship for steel-concrete interface through an inverse analytical method [14].

Results have shown that interfacial cracking occurs at a certain distance from the physical boundary, the interface transition zone; which as stated by the RILEM[15] committee is linked to penetration of cement paste into microstructural rough steel surface. The transition zone is deficient in aggregate content and dominated by the presence of binder due to wall effect [23]. A bimaterial crack hinged model was employed with bilinear softening curve to validate experimental results. However, it is difficult to achieve desirable results with this model, if the interface is not well-posed geometrically or is vulnerable to size effects. Furthermore, there is possibility of plastic zone formation which would lead to stress singularities, that the bilinear softening model is incapable of handling. On the other hand, the method proposed gives us a refined perspective of the crack geometry and strain energy release rate, and being path dependent, it allows us to account for plasticity, branching effects and determining governing failure modes more efficiently. The tension softening at interfaces due to smoothening of surfaces is enforced through an additional crack tip term. Furthermore, the model can be modified to correlate Gibbs energy with the CTOD, for corrosion induced cracks.

CHAPTER 2. ANALYTICAL METHODOLOGY

While significant research effort has focused on developing constitutive and analytical models for brittle-brittle interfaces, damage models and evaluation of fracture toughness parameters for ductile-brittle interfaces remains largely uninvestigated. The cases of out-of-plane strain and in-plane strain for a steady quasi-statically propagating crack between a ductile and brittle material is often expressed through asymptotic near-tip stress and velocity fields; the ductile material is ideally assumed to be plastic characterized by J_2-flow theory with linear hardening while the brittle material is assumed to be linear elastic [16]. Such models implicitly assume the interface to be intrinsically weaker than both materials, which might not be realistic. Due to analytical difficulties associated with obtaining a close formed solution, asymptotic calculations are limited to homogeneous materials, characterized by infinitesimal flow theory. The results suggest the mode-mix of near tip fields maybe unrelated to the combined loading fields and the effect of the far-field is obtained at the crack front through the plastic stress intensity factor [17]. Using an energy based model (as discussed in this thesis), overcomes the computational difficulties associated with near tip stresses and deformation field, by considering the net change in potential energy of the system due to formation of new crack surfaces.

Mathematical representation of interface failure interactions have been primarily described through the lumped and distributed model. In the lumped model, the damage and nonlinearities are confined to an interface of zero thickness; while for the latter, cumulative effects are smeared over a layer of finite thickness. While the actual interface is rough or ribbed due to damaged asperities, the lumped model idealizes it to be smooth. The traction-displacement relationships are expressed through normal and tangential stiffness factors in conjunction with a damage multiplier to generate a non-linear evolution equation defining failure energy for slip to occur by overcoming adhesion [18]. Such cohesive models with linear traction-separation laws are modelled on basis of experimental data and are limited in application. Most practical interfaces present higher resistance than adhesive or friction effects and develop post peak softening or hardening.

Within such limitations, the present work offers an insight towards developing a comprehensive model for ductile-brittle interfaces that is independent of shape effects or geometric asperities at crack tip. Its functionality can be modified to include tension softening/hardening effects for irreversible equivalent strains and size effects. Depending on independently chosen contour paths, computation of the J-Integral would decide the governing failure mode.

The thesis primarily focuses on steel-concrete interface configurations of practical importance subjected to varied loading and failure criterion to depict the versatility of the analytical model.

2.1. Controlled volume fracture model of the steel concrete interface

Path-independent integrals derived from energy conservation laws, are used for determining the intensity of singularity in a field when the exact shape or configuration of the field in the vicinity of crack tip is unknown. They are formulated using a continuously differentiable field whose properties are well-defined in its domain. The benefit of the formulation lies in the fact that if a point singularity exists, the integral can be applied to the domain excluding the singularity making it ideal for computing fracture parameters in spite of dislocation or inclusion defects. The J-Integral is identical to energy release rate for a plane crack extension [1] and it plays the role of an intensity factor for singular stress and strain fields at the crack tip of a power law hardening material [19]. For the model proposed, the quasi static crack propagation is assumed to be time independent and is limited to hyper-elastic materials with stress-free crack borders. Furthermore, the contour integral is incapable of handling bimaterial interfaces especially if it consists of brittle material (concrete) on one side and a ductile surface (steel) on the other. Hence, it is modified to incorporate the strain-hardening post peak plastic response of the steel interface using *Dugdale's (1960)* [20] elasto-plastic fracture model. Although it is well known that steel does not exhibit a complete elasto-plastic behavior, in the proximity of micro cracks the geometric non-linearities can be ignored.

The steel-concrete interface is modelled assuming a negligible interface thickness between them such that fracture energy released in the fracture process zone (FPZ) is a result of overcoming the adhesive forces. Consider an interfacially cracked steel-concrete composite section with thickness t, area A and boundary S, for which the entire volume is controlled.

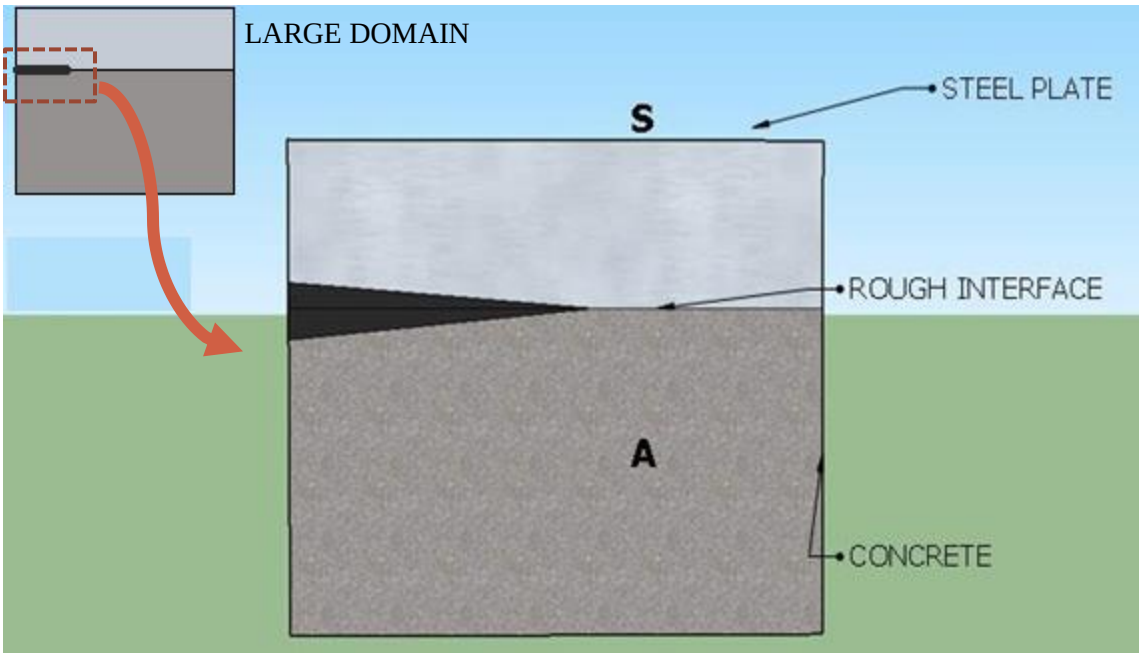

Fig 1. Controlled volume with area A and surface boundary S with rough interface

When this section experiences surface traction T along the boundary S(experimentally simulated by step loading), the potential energy in the controlled volume is given by

$$\Pi=\left[\int_A U\,dA-\int_S T.u\,dS\right]t=\left[\int_A U\,dA-\int_S T_i.u_i\,dS\right]t \qquad (1)$$

where, U:Strain energy density; u:displacement vector.

If the crack is extended by Δa, potential energy of the control volume should also change

Let, PE of the control volume before crack extension: Π_1 and the PE of the control volume after crack extension: Π_2.

The potential energy release rate is then given by

$$-\frac{\partial\Pi}{\partial A}=-\lim_{\Delta a\to 0}\left[\frac{\Pi_2-\Pi_1}{t.\Delta a}\right] \qquad (2)$$

Assuming the module to be part of an infinitely large structure, the potential energies Π_1 and Π_2 can be computed by keeping the crack length fixed and moving the controlled model by the same amount towards the left as the crack propagates towards the right i.e. Δa.

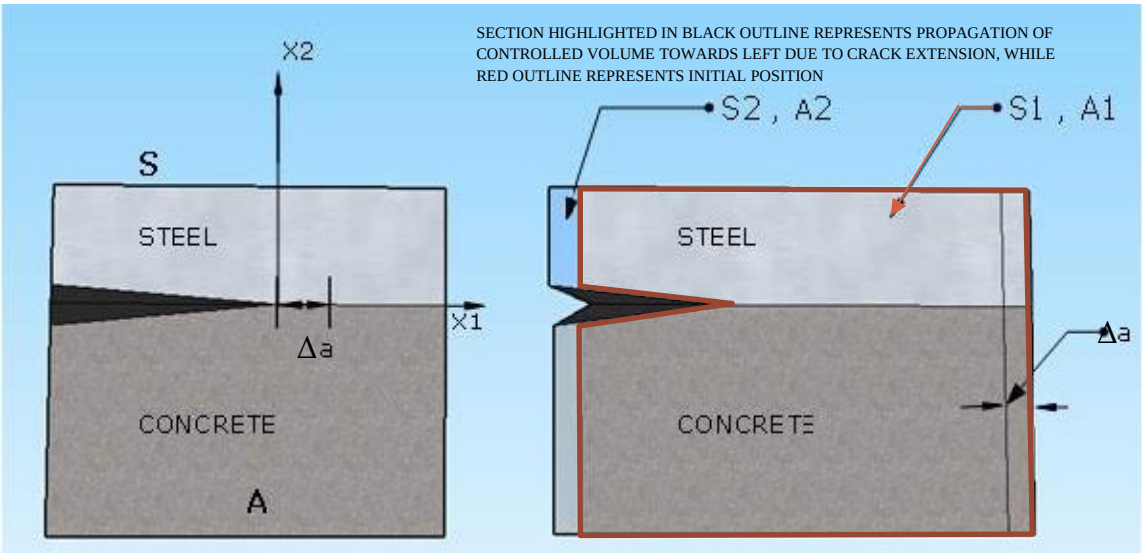

Fig 2. Correlation between displacement of controlled volume and crack tip propagation (as crack propagates towards right the control volume moves towards left)

Before we derive the potential energy release due to crack propagation it is essential to define the nature of the strain energy to be considered for this model. Concrete is a bimaterial, brittle in nature and exhibits catastrophic failure characteristics. The variation of internal energy (δ*E*) stored in a body can be expressed in terms of the variation of strain energy density (δU).

$$\delta E = \int_V \delta U \, dV \tag{2.1}$$

If variation of external work is denoted by δ*W*, it can be related to applied body force (f_i), surface traction (T_i) and variation in displacement as

$$\delta W = \int_V f_i \delta u_i \, dV + \int_S T_i . \delta u_i \, dS \tag{2.2}$$

Hence we can assert that the external work done must be equivalent to the total increment in strain energy of the material.

$$\delta E = \delta W \tag{2.3}$$

$$\int_V \delta U \, dV = \int_V f_i \delta u_i \, dV + \int_S T_i . \delta u_i \, dS = \int_V f_i \delta u_i \, dV + \int_S \sigma_{ij} n_j . \delta u_i \, dS \tag{2.4}$$

After performing necessary substitutions and applying Gauss divergence theorem;

$$\int_V \delta U \, dV = \int_V f_i \delta u_i dV + \int_V (\sigma_{ij} \delta u_i)_{,j} dV = \int_V (f_i \delta u_i + \sigma_{ij,j} \delta u_i + \sigma_{ij} \delta u_{i,j}) dV \tag{2.5}$$

Since, $\sigma_{ij,\,j} + f_i = 0$, the preceding equation can be simplified as

$$\int_V \delta U \, dV = \int_V (\sigma_{ij} \delta u_{i,j}) dV = \int_V \frac{1}{2} (\sigma_{ij} \delta u_{i,j} + \sigma_{ji} \delta u_{j,i}) dV = \int_V \sigma_{ij} \delta \epsilon_{ij} dV \tag{2.6}$$

Hence, $$\delta U = \sigma_{ij} \, \delta \varepsilon_{ij} \tag{3}$$

From Eq(3), the stress strain relation can be obtained by assuming relevant expression of U_0 in terms of strain components applying Green's approach (say, if we assume the strain energy density to be a quadratic function, then $U = D_0 + D_{kl} \, \varepsilon_{kl} + D_{klmn} \, \varepsilon_{kl} \, \varepsilon_{mn}$). But for our model we prefer to stay in the linear elastic fracture mechanics domain, for which we assume a linear strain energy density which gives a linear stress-strain relation $\sigma_{ij} = D_{ijkl} \, \varepsilon_{kl}$. From the above expression it is clear that we can express U as area under the linear $\sigma - \varepsilon$ curve, which may be obtained from experimental data.

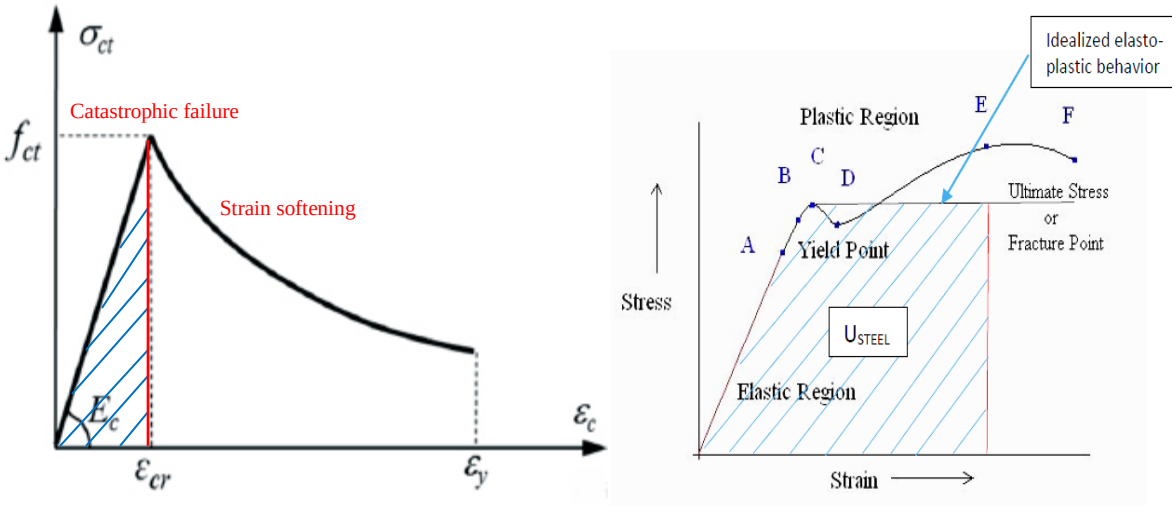

Fig 3. Stress-strain relation for concrete and steel assumed at interface to obtain strain energy

2.2. Application of J-Integral to interface crack propagation

Even though the contour integral was originally proposed to be one dimensional, it can be reformulated as an area or volume integral using the Gauss Divergence Theorem for 2D and 3D configurations over a finite domain enclosing the crack tip. The shift of crack front advance is assumed to be perpendicular to the crack plane normal for 2D cases and the crack front tangent for 3D cases where the front intersects the external surface of the solid. The value of J-integral associated with a fictitious small crack advance, along any path within the process zone with no singularities is zero or constant, as long as the path is around one end of the crack tip. Stability and symmetry conditions are limited to static processes and hence only constant body forces like gravitation, which have potential without explicit dependence on crack growth, can be considered for computing external work to maintain path independence. Also, the crack faces are required to be traction free. The path independence property allows us to freely investigate the crack path propagating along the interface or straying away from it. We can ignore contours close to the crack tip

where the displacement and stress fields are difficult to compute accurately owing to stress singularities or presence of a plastic zone, and choose a remote path along the boundaries or symmetry points of the domain on which the tractions and strain energies can be deciphered with relative simplicity.

The possible integration path is $\Gamma = abcdefg$. Considering integral direction in the counter-clockwise sense we get, $\Gamma' = \Gamma - \Gamma_{gd} - \Gamma_{da}$. Now, Eq(2) can be written as

$$-\frac{d\Pi}{dA} = -\lim_{\Delta a \to 0} \frac{1}{t\Delta a}\left[\left(\int_{A_2} U\,dA - \int_{S_2} T_i u_i\,dS\right) - \left(\int_{A_1} U\,dA - \int_{S_1} T_i u_i\,dS\right)\right] t \quad (4.1)$$

Fig 4. Remote integral path for obtaining J-Integral at the steel-concrete interface

The potential energy released by the system due to extension of the crack front is a result of the exchange of stresses and tractions at the interface. Hence, in the succeeding

equations, the strain energy densities and traction slip parameters have been disintegrated into components to enforce contribution of both materials towards crack propagation.

$$-\frac{d\Pi}{dA} = -\lim_{\Delta a\to 0}\frac{1}{t\Delta a}[\left(\int_{A_2} U_c\,dA - \int_{S_2} T^2_{i,c}u^2_{i,c}\,dS + \int_{A_2} U_s\,dA - \int_{S_2} T^2_{i,s}u^2_{i,s}\,dS\right) - \left(\int_{A_1} U_c\,dA - \int_{S_1} T^1_{i,c}u^1_{i,c}\,dS + \int_{A_1} U_s\,dA - \int_{S_1} T^1_{i,s}u^1_{i,s}\,dS\right)]t \tag{4.2}$$

$$-\frac{d\Pi}{dA} = \lim_{\Delta a\to 0}\frac{1}{\Delta a}\left[\underbrace{\int_{A_1-A_2}(U_c+U_s)\,dA}_{SERR\ 1} + \underbrace{\int_{S_2}(T^2_{i,c}u^2_{i,c}+T^2_{i,s}u^2_{i,s})\,dS - \int_{S_1}(T^1_{i,c}u^1_{i,c}+T_{i,s}u^1_{i,s})\,dS}_{SERR\ 2}\right] \tag{4.3}$$

where, SERR 1: Strain energy release rate due to preferential interfacial crack

SERR 2: Strain energy release due to traction slip.

Using LEFM; for the limiting case ($\Delta a\to 0$); we can assume the displacement field to vary linearly between S_1 and S_2. For small regions u can always be assumed to be varying linearly even for non-linear displacement fields as long as there is no discontinuity. Furthermore; the traction, stress and strain fields should also be constant for linear displacement fields. Hence, we can safely state:

$$T^1_{i,c} = T^2_{i,c} = T_{i,c} \quad T^1_{i,s} = T^2_{i,s} = T_{i,s}$$

Also, since the displacement field for both steel and concrete are same at the boundaries S_1 and S_2, we assume

$$u^1_{i,c} = u^1_{i,s} = u^1_i \quad u^2_{i,c} = u^2_{i,s} = u^2_i$$

Eq(4.3) can therefore be expressed as

$$-\frac{d\Pi}{dA} = \lim_{\Delta a \to 0} \frac{1}{\Delta a} \left[\int_{A_1 - A_2} (U_c + U_s)\, dA + \int_S T_{i,c}(u^2_{i,c} - u^1_{i,c})\, dS + \int_S T_{i,s}(u^2_{i,s} - u^1_{i,s})\, dS \right]$$

$$= \lim_{\Delta a \to 0} \frac{1}{\Delta a} \left[\int_{A_1 - A_2} (U_c + U_s)\, dA - \int_S (T_{i,c} + T_{i,s})(u^1_i - u^2_i)\, dS \right] \tag{5}$$

From Eq(5) we are able to correlate the total strain energy released for the interface $U^T = U_c + U_s$ and net traction $T_i = T_{i,c} + T_{i,s}$ with the potential energy release rate, which will be applied in succeeding equations. Since S_1 and S_2 are separated by Δa, displacement field on the two boundaries are related as

$$u_i^{(1)} = u_i^{(2)} + \frac{\partial u_i}{\partial x_i} \Delta a \tag{6}$$

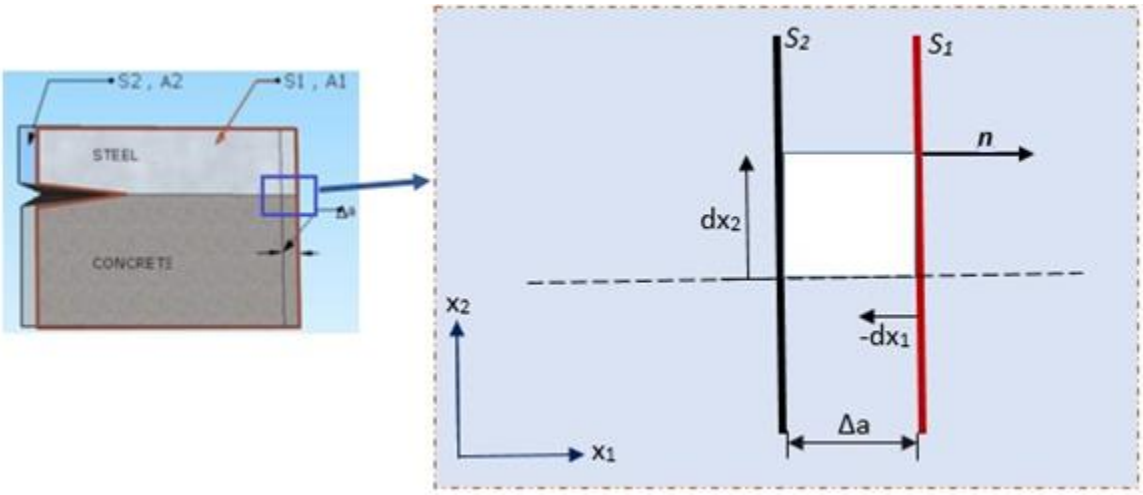

Fig 5. Elemental area enclosed by boundaries S_1 and S_2 separated by Δa

From Eq(5) and Eq(6)

$$-\frac{d\Pi}{dA} = \lim_{\Delta a \to 0} \frac{1}{\Delta a} \left[\int_{A_1 - A_2} U^T\, dA - \left(\int_S T_i (u_i^{(1)} - u_i^{(2)})\, dS \right) \right]$$

$$= \lim_{\Delta a \to 0} \frac{1}{\Delta a} \left[\int_{A_1 - A_2} U^T\, dA - \left(\int_S T_i \frac{\partial u_i}{\partial x_i} \Delta a\, dS \right) \right] \tag{7.1}$$

From Fig 5. we observe that elemental area $dA=\Delta a.dx_2$. Substituting in Eq(7.1)

$$-\frac{d\Pi}{dA} = \lim_{\Delta a \to 0} \frac{1}{\Delta a} \left[\int_{A_1 - A_2} U^T \, \Delta a.dx_2 - \left(\int_S T_i \frac{\partial u_i}{\partial x_i} \Delta a \, dS \right) \right]$$

$$= \int_S U^T \, dx_2 - \int_S T_i \frac{\partial u_i}{\partial x_i} \, dS = \int_S \left(U^T \, dx_2 - T_i \frac{\partial u_i}{\partial x_i} \right) \, dS \tag{7.2}$$

At the interface $S_1=S_2=S$ and since the total strain energy is equivalent to the external work done the J-Integral is given by

$$J_{\Gamma \to abcdefg} = \int_S W dx_2 - \int_S T_i \frac{\partial u_i}{\partial x_i} dS \tag{7.3}$$

$J_{\Gamma \to abcdefg}$=SERR–Tangential traction slip energy for steel–concrete interface (8)

Eq(8) considers the gross potential energy change or fracture energy release due to the system as a whole. However we are concerned about the interface itself. The J-Integral for net fracture energy release into the process zone at interface is given by

$$J_{interface} = J_{\Gamma \to abcdefg} - J_{gd} - J_{da} \tag{9}$$

where ,

$$J_{da} = \int U_{conc} dx_2 - \int_{da} T^{conc} \frac{\partial u_2^{conc}}{\partial x} dS \tag{9.1}$$

$$J_{gd} = \int U_{steel} dx_2 - \int_{gd} T^{steel} \frac{\partial u_2^{steel}}{\partial x} dS \tag{9.2}$$

2.3. Modified fracture model to consider plasticity effects at the interface crack tip and impinging effect

When hard brittle and ductile metal surfaces come into contact at asperity tips; the asperities notch into the metal surface causing it to yield plastically due to local stress concentrations when coupled with diffusional mass transfer, leading to shrinkage of interfacial voids, allowing the crack tip to propagate. Severe restrictions for J-results can be attributed to existence of strain energy density which uniquely defines the potential for deriving stresses. The irreversible plastic deformations, local unloading processes, and stress rearrangements are concealed from the results. Moreover, for non-homogeneous stress fields, if the loading is monotonically increasing instead of being pseudo-static, it does not sufficiently guarantee radial stress paths making the J-integral path dependent with the onset of plasticity. The expressions derived above do not account for the plastic zone due to the ductile stretch of the steel interface at the crack tip. For small scale yielding, the J-Integral can be computed outside the plastic zone if the domain under evaluation is large enough to cover the plastic zone and passes through the elastic region. The problem can be addressed by choosing an integral path about the plastic zone for a Dugdale type plasticity model.

J-integral is carried out on $S=S_{steel}US_{concrete}$. The path independence is valid as long as the material enclosed between the two boundaries is elastic. Since the interface is inelastic, the equivalence of the strain energy release rate to the J-Integral is invalid in such a scenario i.e. ($J \neq SERR$). But, J can still be calculated for the problem geometry and equated to the crack tip opening displacement (CTOD). Extending Eq(8) to incorporate plasticity effects:

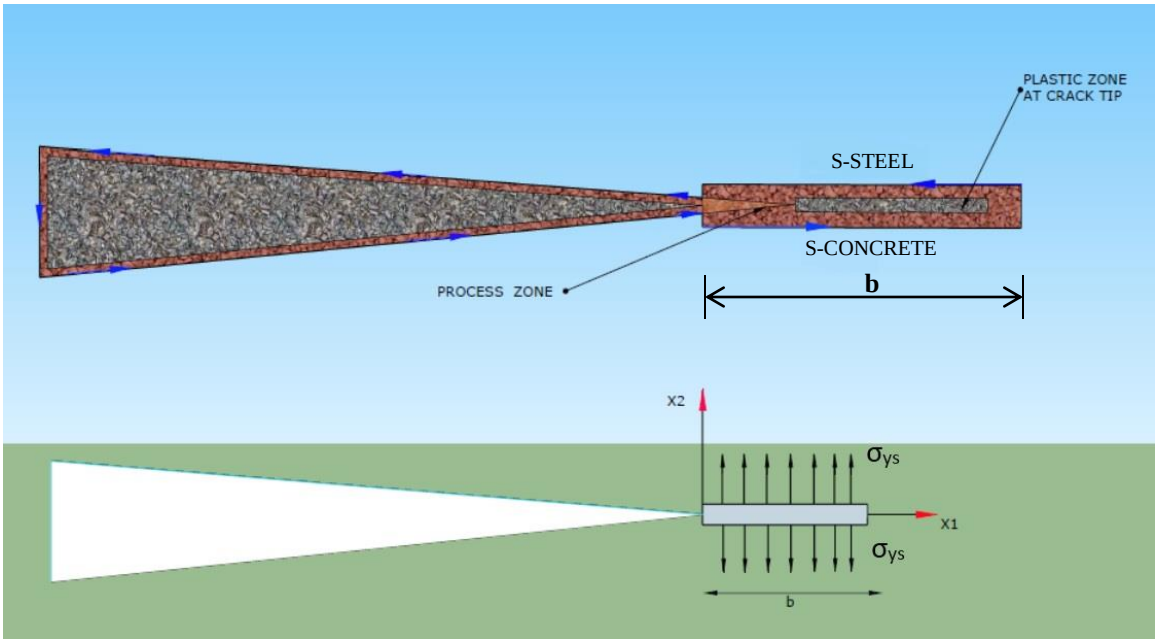

Fig 6. (a)Contour surrounding the plastic zone: Dugdale model (b)Stresses and traction fields surrounding plastic zone

$$J = \int_{S^{conc}} \left(U_{conc}\, dx_2 - T_i \frac{\partial u_i}{\partial x_i} dS \right) - \int_{S^{steel}} \left(U_{steel}\, dx_2 + T_i \frac{\partial u_i}{\partial x_i} dS \right) \tag{10}$$

From Fig 6. the boundary interface path for the integral path can be specified as

$$S = \begin{cases} \textbf{on lower path} & S^{conc}: T = -\sigma_Y \;\; ds = dx_1; dx_2 = 0 \\ \textbf{on upper path} & S^{steel}: T = +\sigma_Y \;\; ds = dx_1; dx_2 = 0 \end{cases}$$

where, σ_Y represents the yield stress at crack tip.

The subsequent equations facilitate an arbitrary shift of the crack front yielding the energy release rate towards the plastic zone. Hence Eq(10) can be expressed as

$$J = \int_0^b \left(U_{conc} x\,0 - T_i^{conc} \frac{\partial u_i^{conc}}{\partial x_1} dx_1 \right) - \int_0^b \left(U_{steel} x\,0 + T_i^{steel} \frac{\partial u_i^{steel}}{\partial x_1} dx_1 \right) \tag{10.1}$$

$$= - \int_0^b T_{conc} \frac{\partial u_{conc}}{\partial x_1} dx_1 - \int_0^b T_{steel} \frac{\partial u_{steel}}{\partial x_1} dx_1 \tag{10.2}$$

$$=\sigma_Y \left[\int_0^b \frac{\partial (u_{conc} - u_{steel})}{\partial x_1} dx_1 \right] \tag{10.3}$$

$$=\sigma_Y \left[u_{conc} - u_{steel} \right]_0^b = \sigma_Y [CTOD - 0] \tag{10.4}$$

Hence, the J-Integral can be related to the elasto-plastic crack tip opening displacement

$$\mathbf{J = \sigma_{Yield} \, x \, CTOD} \tag{11}$$

For large plastic deformations; it should be kept in mind that J being a monotonically increasing function of the distance from crack tip, crack propagation would lead to energy production instead of dissipation thereby violating the second law of thermodynamics. The saturated J value with a incremental domain is always the nearest to the 'real' far field J [21]. The strain energy release ratio for cracks at the interface depends on the angle at which the crack propagates as well as the material properties.

It is possible, that a given crack might find itself energetically favorable to branch off the interface and penetrate into either the brittle or ductile media unless the interface itself is weaker than either phase [16]. The J-integral for cracks emanating at multiple angles from the crack tip into the material microstructure can provide us with insight regarding the variation of SERR at the interface and the minimum energy which defines the failure path. In order to account for impinging effects, the integral path is not allowed to cross the interface as the fracture parameters would be uni-materialistic for such cases. *Shansuo et al.*[22] was able to generate curves for variation of J-Integral with θ. Using curve fitting techniques, they were able to arrive at an expression connecting the fracture energy released by the existing crack to the impinging crack.

$$G_{imp}=G_{exist}\exp(w\theta^3) \quad ;w=f\left(\frac{d}{a}\right) \tag{12}$$

Where, G_{imp}: Fracture energy of impinged crack, G_{exist}: Fracture energy of existing curve, d:impinged crack length, a: length of branching crack front

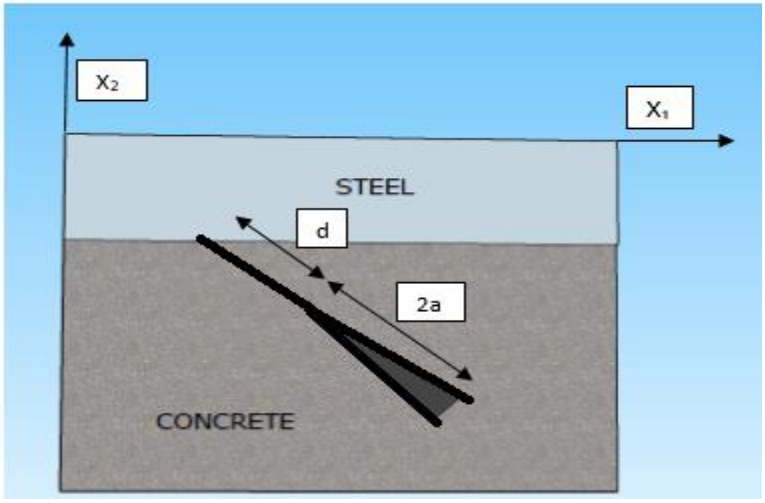

Fig 7. Impinging of cracks near the interface

From the empirical formulation; it can be concluded that the strain energy released into the process zone depends on the increasing angle between the impinging crack path and interface.

2.4. Empirical evaluation of fracture toughness parameters and stress intensity factors

The fracture toughness of matrix-aggregate interface for mixed mode failure was obtained by modifying Dundur's [11] parameters (α and β) which can be stated as [10]

$$\alpha = \frac{\bar{E}_1 - \bar{E}_2}{\bar{E}_1 - \bar{E}_2} \quad , \quad \beta = \frac{1}{2}\frac{\mu_1(1-2\nu_2) - \mu_2(1-2\nu_1)}{\mu_1(1-\nu_2) + \mu_2(1-\nu_1)}$$

However in order to evaluate mixed mode fracture toughness parameters K_I, K_{II} for the steel-concrete bimaterial interface, we can use Shih, Asaro's(1989)[19] model which

considers a periodic array of cracks and prescribes an adhesive relation that governs the normal and shear displacement response. Assuming ψ to be the loading phase angle (which is a measure of the shearing displacement or slip to the opening or normal displacement at the steel concrete interf the coupled SIF's for mode I and II under far field tensile stress σ_{22}^{∞} and shear stress σ_{12}^{∞}, can be stated as

$$K_I+iK_{II}=(\sigma_{22}^{\infty}+i\sigma_{12}^{\infty})(1+2i\varepsilon)\sqrt{\pi\frac{L}{2}}L^{-i\varepsilon} \tag{13}$$

where,

$$\varepsilon=\frac{1}{2\pi}\ln\frac{\frac{3-4\mu_c}{\mu_c}+\frac{1}{\mu_s}}{\frac{1}{\mu_c}+\frac{3-4\mu_s}{\mu_s}}$$

The SERR for the plane strain case (Xiong et al.2010[13]) is given as

$$G_I+G_{II}=\frac{(K_I^2+K_{II}^2)\left(\frac{1-\nu_c}{\mu_c}+\frac{1-\nu_s}{\mu_s}\right)}{4\cosh^2(\pi\varepsilon)}$$

$$K_I^2+K_{II}^2=\frac{2\mu_n}{1-\nu_n}(G_1^n+G_2^n)\ ;\ n=1,2,\cdots \tag{14}$$

In the above expression; *L* represents the total length of the crack. μ and ν represent the shear modulus and Poisson's ratio respectively. ε is constant for the interface and is predicted to be less than 0.1.

CHAPTER 3. ILLUSTRATIVE APPLICATIONS

3.1. Fracture of the shear connector-microstructure-steel plate interface

Steel-concrete(SC) composite walls are of great importance to the nuclear energy industry. It consists of a concrete wall connected to steel plates using shear connectors and tie rods at well-defined intervals. The steel plate with the connector elements serve as the formwork for the concrete poured. While a significant amount of research has been performed on the assessment of local and global failure modes for SC walls, the fracture origination, propagation and branching at the interface level is yet to be investigated. This thesis aims at identifying the possible interfaces of the basic SC wall module and establishes LEFM techniques with inclusion of certain non-linear parameters, to shed light on certain major fracture parameters that govern the failure of its components.

3.1.1 Modified J-Integral model to compensate for tension softening and singularity at crack tip

The previous sections dealt with the failure of the steel plate-concrete interface assuming an adhesive bond between the two rough interfaces. However, for an SC wall the primary failure mode is governed by the slipping of the shear connector elements. However, tensile yielding of steel or compressive crushing of concrete are probable failure modes as well. In order to maintain continuity in analysis, we would be using the J-Integral

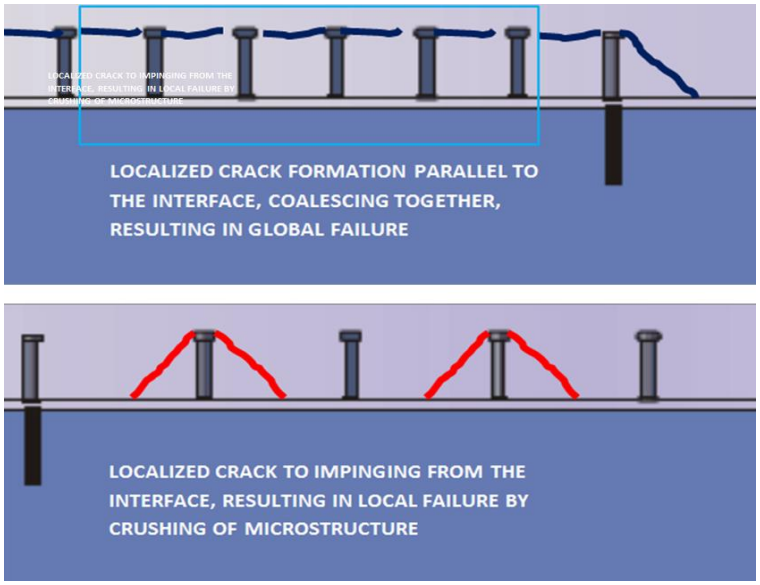

Fig 8. Failure modes for the stud-concrete-steel plate interface

along a probabilistic failure path the crack tip is likely to follow. However, it is essential to note that unlike the elasto-plastic nature of the steel-concrete interfacial crack tip propagation; the stud would exhibit a post-peak softening behavior which would require us to bridge Rice's model to some additional crack tip parameters. Lastly, we wish to delocalize the shearing or slip effect of the stud to the surrounding concrete microstructure which requires us to smear the fracture energy across the interface. Hence, there is no well-defined crack tip opening when the slip or tearing of the shear connector occurs, due to the fact that the localized energy around the fracture process zone would cause crushing of the surrounding concrete.

The J-integral has been widely used to generalize fracture toughness of ductile and quasi-brittle materials, and is a well-accepted parameter for stress intensity and energy supply characterization. When stress rearrangements occur at the deforming tip, J maintains a finite value in the limit of a diminishing contour as long, as the strain energy density in the vicinity of the crack tip has a singularity of the order -1. If the

unloading of a specimen follows the identical stress-strain path as its loading phase, such non-linear elastic behavior can be justified by the path independence of the J-Integral. But, in this case, the material develops tension softening leading to growth of FPZ by interlinking propagating crack flanks. The confusion in applying the J-integral to such materials arises during evaluation of the contour surrounding the process zone, when the unloading of the material defies the non-linear elastic assumption behind the basic J-Integral formulation [23]. The issue is addressed by considering a contour Γ_{remote} far from the FPZ that passes through the concrete microstructure and the steel plate. Due to path independence of the J-integral the contour Γ_{pz} wrapped around the fracture process zone possesses the same value as Γ_{remote}. When the material enclosed by the process zone unloads elastically with decreasing tensile traction σ and increasing crack opening (on the line y=0) δ; the material at the process zone(Γ_{pz}, $y=0^{+}\cup 0^{-}$) must also unload in order to maintain equilibrium, which is elastic in nature and follows the traditional stress-strain relationship [23]. The remote contour in conjunction with the contour wrapped around the process zone allows us to determine the correlation between energy released and supplied during tension softening. In our case, a bridging model seems feasible that would result in a correction term, in addition to the integral; when the additional contour wrapped around the crack tip shrinks, which is similar to the cohesive crack model.

$$J=\frac{K_{tip}^{2}(1-\nu^{2})}{E}+\int_{0}^{\delta t}\sigma(\delta)d\delta \tag{23}$$

where, $\sigma(\delta)$: describes the tension softening of the process zone; $K_{tip} \Rightarrow$ fracture toughness; E: Elastic modulus; ν: Poisson's ratio; δ_t: crack tip opening at end of the fracture process zone. Critical value of the integral ($J=J_{crit}$) occurs when the traction free crack opening $\delta_t \rightarrow \delta_{crit}$ corresponding to $\sigma_{crit}=0$. Energy consumed in the process zone is comparatively greater than at the advancing crack tip. The empirical expression for $\sigma(\delta)$ for concrete under uniaxial tension was given by Stang et al.(1992)[50]

$$\sigma(\delta)= \frac{\sigma_m^u}{1+\frac{\delta_P}{\delta_0}} \quad ; \sigma_m, \delta_p \text{ and } \delta_o \text{ are empirically determined}$$

3.1.2 Application of J-Integral for crack path propagation due to slip of steel plate

We follow a similar procedure as applied to the steel plate concrete interface and try to use the path independence property to avoid crack tip singularity by calculating stresses and tractions along the remote contour, when the stud is exposed to slip forces. Three possible integral paths can be defined for cracks propagating parallel to the interface

Γ=LABCDEFGHIJKL ;defining the entire domain

Γ_C=IJLKA=Γ_{remote} ;defining the far field integral path in concrete microstructure

Γ_S=IAKMJ ;defining the integral path in steel

Γ_{pz}=IHGFEDCBA; integral path in fracture process zone where crack originates and branches out

We can correlate the integral paths and incorporate the different phases of fracture propagation using the expression

$$\Gamma=\Gamma_{remote/conc}+\Gamma_{steel}-\Gamma_{stud}$$

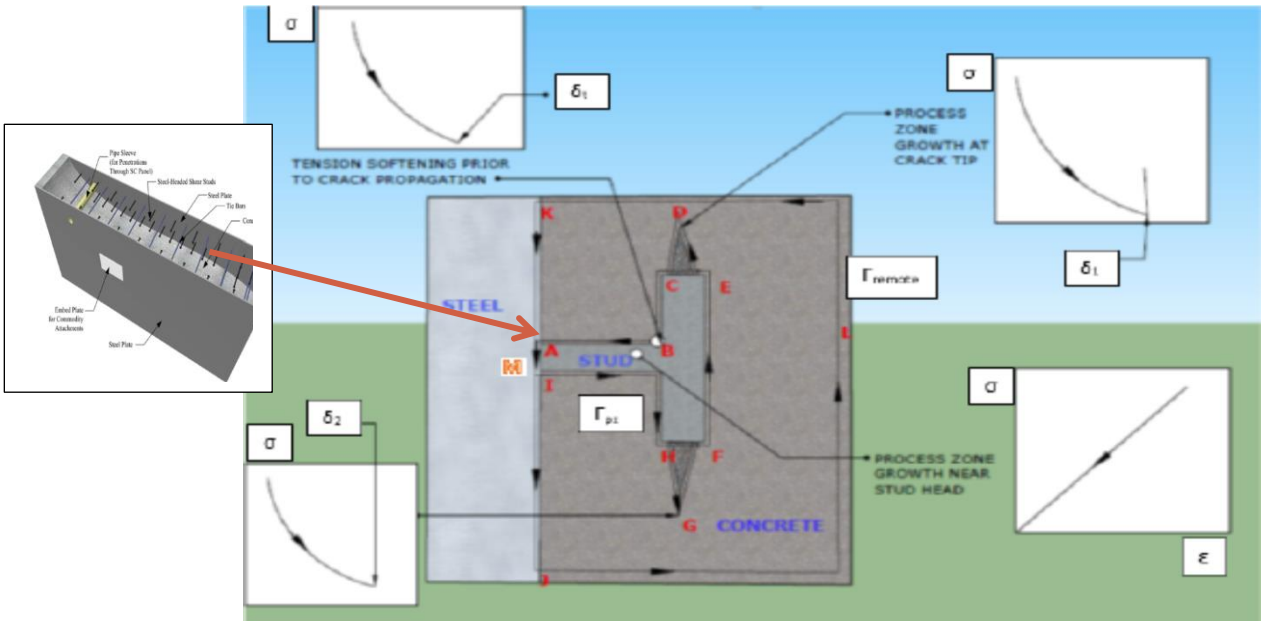

Fig 9. Integral paths defined at the process zone to capture inelastic tension softening effects at stud-concrete-steel plate interface

Now, from the definition of J-integral, where δ_1 and δ_2 are smeared crack tip opening parallel to the interface, we obtain (from Eq 7.3 obtained in Chapter.2)

$$J_{conc/remote} = \int_{\Gamma_{conc}} W^{conc} dy - \int_{\Gamma_{conc}} T^{conc} \frac{\partial u^{conc}}{\partial x} dS \; ; S \rightarrow S_{conc} \tag{15}$$

$$J_{steel} = \int_{\Gamma_{steel}} W^{steel} dy - \int_{\Gamma_{steel}} T^{steel} \frac{\partial u^{steel}}{\partial x} dS \; ; S \rightarrow S_{steel} \tag{16}$$

$$J_{stud} = \int_{\Gamma_{stud}} W^{stud} dy - \int_{\Gamma_{stud}} T^{stud} \frac{\partial u^{stud}}{\partial x} dS + \frac{K_{tip}^2 (1-\nu^2)}{E} \tag{17}$$

Using Eq 23; bridging the integral with crack tip correction term

$$= \int_0^{\delta_T} \sigma(\delta) d\delta - \int_{\Gamma_{stud}} \underbrace{T^{stud}}_{Slip\ traction} \frac{\partial u^{stud}}{\partial x} dS + \frac{K_{tip}^2 (1-\nu^2)}{E} \; ; S \rightarrow S_{stud} \tag{18}$$

Dissociating the integral for crack fronts CDE and HGF, we obtain

$$J_{stud} = \left(\int_{\Gamma_{CDE}} \sigma(\delta) d\delta_1 + \int_{\Gamma_{HGF}} \sigma(\delta) d\delta_2 \right) - \int_{\Gamma_{stud}} T^{stud} \frac{\partial u^{stud}}{\partial x} dS + \frac{K^2_{tip}|_{CDE}(1-\nu^2)}{E} + + \frac{K^2_{tip}|_{HGF}(1-\nu^2)}{E} \quad (19)$$

The expression for process zone satisfies the stress and displacement continuity. The singularity in the process zone due to tension softening is taken care of by the additional crack tip term. However, it is important to observe that we are neglecting plasticity effects at the crack tip as experiments have proven that the size of plastic zone during slip of shear stud is meager compared to the softening phase.

3.2. Application of J-Integral for stud-microstructure interface due to pullout

When subjected to pullout forces the stud experiences local buckling at the connector-steel plate-concrete interface and the crack is expected to follow a path propagating at an angle from the crack tip causing local (micro-meso) failure and crushing at the base of stud. The nature of failure is opposed to the scenario when the steel plate is subjected to slip; where the cracks from stud tip branch out and coalesce resulting in a global (macro-meso) failure and debonding of the concrete chunk (see Fig. 8).

The probable integral paths for cracks propagating at an angle of θ from the crack tip can be defined as

Γ =ahgfponmk

Γ_C =onml=Γ_{remote}

Γ_S =hgfpolka

Γ_{pz} =gjfedcbaih

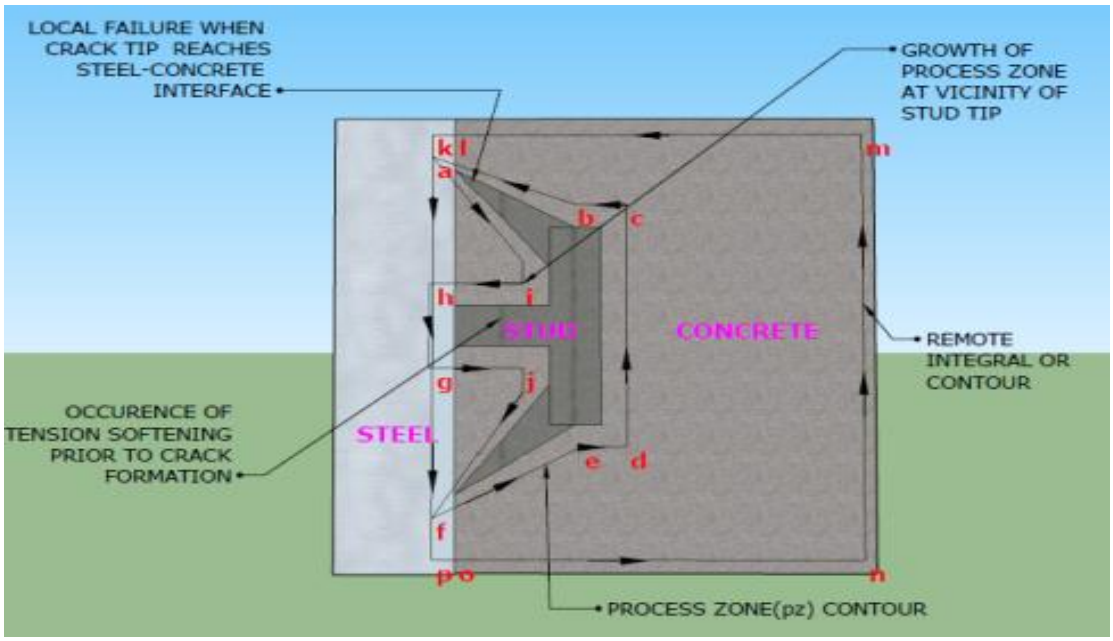

Fig 10. Integral path for the stud-concrete-steel plate interface when subjected to pullout forces

$$\Gamma = \Gamma_{remote/c} + \Gamma_s - \Gamma_{pz}$$

The failure resistance is the resultant of tensile stresses equal to maximum concrete tensile strength directed perpendicular to the conical plug surface resulting from pullout forces at an angle of 25 degrees (for shallow embedments) to 45 degrees (for deep embedments) and parallel to the direction of applied load [24] . The stresses are not directed towards the major axes. Hence we need to take components of the principal stresses at the fracture process zone along the predicted crack path propagation.

From path independence of J-Integral we can assert $\Gamma_{abcdef}=\Gamma_{klmnop}$ and $\Gamma_{aihgjf}=\Gamma_{kpol}$.

$$J_{conc/remote} = \int_{\Gamma_{conc}} W^{conc} dy - \int_{\Gamma_{onml}} T^{conc} \frac{\partial u^{conc}}{\partial x} dS \; ; S \rightarrow S_{conc} \qquad (20)$$

$$J_{steel} = \int_{\Gamma_{steel}} W^{steel} dy - \int_{\Gamma_{ahgfpolk}} T^{steel} \frac{\partial u^{steel}}{\partial x} dS \; ; S \rightarrow S_{steel} \qquad (21)$$

$$J_{stud} = \int_{\Gamma_{stud}} W^{stud} dy - \int_{\Gamma_{stud}} T^{stud} \frac{\partial u^{stud}}{\partial x} dS + \frac{K_{tip}^2 (1-\nu^2)}{E} \tag{22}$$

Using Eq 23; bridging the integral with crack tip correction term

$$= \int_0^{\delta_T} \sigma(\delta) d\delta - \int_{\Gamma_{aihgjfedcb}} \underbrace{T^{stud}}_{Slip\ traction} \frac{\partial u^{stud}}{\partial x} dS + \frac{K_{tip}^2 (1-\nu^2)}{E}; S \to S_{stud} \tag{23}$$

Using the path dependence relations,

$$J_{stud} = \left(\int_{\Gamma_{aihgjf}} \sigma(\delta) d\delta_1 + \int_{\Gamma_{cdefponmlk}} \sigma(\delta) d\delta_2 \right) - \underbrace{\int_{\Gamma_{stud}} T^{stud} \cos\theta \frac{\partial u^{stud}}{\partial x} dS_{pz}}_{normal\ traction\ component} - \underbrace{\int_{\Gamma_{stud}} T^{stud} \sin\theta \frac{\partial u^{stud}}{\partial x} dS_{pz}}_{shearing\ traction\ component} + \frac{K_{tip}^2|_{jfe}(1-\nu^2)}{E} + \frac{K_{tip}^2|_{iab}(1-\nu^2)}{E} \tag{24}$$

where δ_1 and δ_2 are smeared crack displacements and θ is angle of the crack to the horizontal plane.

3.3. Size effect on fracture energy release into process zone

Bazant et al.[25] examined the quasi-brittle nature of shear connectors with post-peak softening and also analyzed the size effect on nominal strength of composite beams. However, it is expected that the post-peak softening will increase with the size of stud[25]. Since the studs do not reach their maximum shear strength simultaneously, the crack propagates parallel to the interface, which requires energy release analysis.

According to the approximate theoretical energy model, the shear flow(T) vs. slip(v) is a piecewise linear function; in which the shear force initially increases without any slip for the first loading as shown in Fig. 10(a). However, for repeated loading the initial adhesive bonding vanishes and the T vs. v relation develops a finite slope. The second

line segment corresponds to a simplified linear incremental shear flow leading to a peak value, the third represents post-peak softening. The tension softening also depends on the size of plastic zone (see Fig 10(b)). The last phase depicts frictional slip at a constant stress equivalent to the residual shear strength

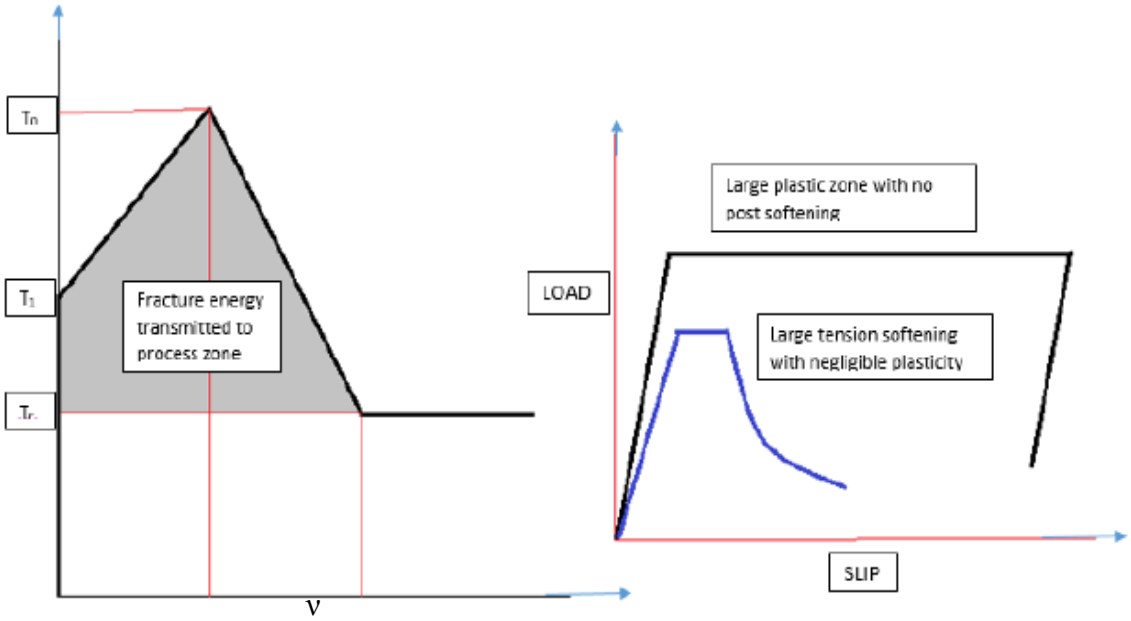

Fig 11. (a)Idealized shear force-slip diagram for deformable connectors [18](b)Idealized plastic zone formation and post peak tension softening

The post-peak decrease of stud force or softening localizes into a finite zone called the fracture process zone. Also, the limit capacity is not reached simultaneously in all the connectors as assumed in plastic analysis; but only to a limited group of connectors that occupy a finite length. and propagates due to loading at the steel-concrete interface. Since, softening is defined by stress-displacement relation rather than the stress-strain relation, the crack length is approximately constant.

3.4. Microstructural damage of the reinforcement-concrete interface when subjected to pullout forces

The bond slip and anchorage length determination of reinforcement embedded in concrete is a complex phenomenon. The ACI 318[26] code gives simple provisions for defining the development length of reinforcing bars considering average bond resistance over the entire anchored length, so that the bar can develop its complete yield capacity. However, the anchorage length for a single bar and multiple bars vary owing to a weak plane formation due to splitting cracks. The code also incorporates empirical correction factors such as c_b(smallest side cover), K_{tr}(contribution of confining reinforcement along splitting planes), ψ_t(location factor); but doesn't speak about the mechanics of debonding and crack propagation at the interface level. Furthermore, the development length is obtained on the basis of plastic shear slip behavior by equating the reinforcement yield load ($F_y=A_s*f_y$) to bond strength ($\tau_c(2\pi r)*L_s$); τ_c being the critical shearing force and r, L_s the radius and slip distance, respectively. A linear proportionality can be developed between these parameters, concrete strength (f'_c) and the tensile splitting strength (f'_t) as

$$\tau_c \propto f'_t \propto \sqrt{f'_c}$$

from which the development L_d can be expressed as $CA_s f_y/\sqrt{f'_c}$; C being an empirical constant derived from experimental data.

The thesis tries to define a theory based on fundamental NLFM and EPFM concepts to answer questions pertaining to the local and global failure modes of the interfacial rebar fracture. Ingraffea et al.[27] used a cohesive non-linear fracture model to account for tension softening behavior and concluded that secondary cracking emanating from the

primary cracks leads to slipping. Bazant *et al.*[28] used axis-symmetric formulations in accordance with circumferential stress-strain relationship for a smeared cohesive model to obtain a simplistic crack softening function.

This study tries to build a simplistic model of the rebar pullout phenomenon by subdividing it into three zones based on interfacial parameters, aggregate interlock, cohesion and formation of plastic and tension softening regions due to confined concrete. Once again, the path independent J-Integral is used for obtaining the fracture energy taking into consideration Li's tension softening model[23] in conjunction with Bazant's strain-softening function[28].

3.4.1. Elasto-plastic fracture model for rebar specimen embedded in concrete

We divide the specimen into three primary zones as mentioned above according to their failure criterion. Zone I represents the formation of conical plug at the pullout face while Zone II depicts crushing where the concrete bears on steel ribs and Zone III represents the crushing of confined concrete at the base. Ingraffea et.al[27] rightly asserted secondary cracking to be the dominant mechanism contributing to slip. LEFM concepts cannot be applied to short crack lengths associated with bond slip.

The Zone I crack is explained using Dugdale's plasticity model. The expression for J-Integral can be given by

$$J = \int_{S_1} \left(U\,dx_2 - T_i \frac{\partial u_i}{\partial x_i} dS \right) - \int_{S_2} \left(U\,dx_2 + T_i \frac{\partial u_i}{\partial x_i} dS \right) \tag{25}$$

From Fig.12, we obtain

$$S = \begin{cases} \text{on lower path} & S_1 : T = -\sigma_Y \;\; ds = dx_1 ; dy = dx_2 \\ \text{on upper path} & S_2 : T = +\sigma_Y \;\; ds = dx_1 ; dy = dx_2 \end{cases}$$

where, σ_Y is yield stress at the lug crack front

$$J = \left(\int_0^{b\sin\theta} U\,dx_2 - \int_0^{b\cos\theta} T_i \frac{\partial u_1}{\partial x_1} dx_1 \right) - \left(\int_{b\sin\theta}^{0} U\,(dx_2) - \int_{b\cos\theta}^{0} T_i \frac{\partial u_2}{\partial x_1} dx_1 \right) \quad (26)$$

$$= \begin{pmatrix} b\sin\theta & 0 \\ \int U dx_2 - & \int U(dx_2) \\ 0 & b\sin\theta \end{pmatrix} + \begin{pmatrix} b\cos\theta & b\cos\theta \\ - \int T_1 \frac{\partial u_1}{\partial x_1} dx_1 - & \int T_2 \frac{\partial u_2}{\partial x_1} dx_1 \\ 0 & 0 \end{pmatrix} \quad (27)$$

$$= \begin{pmatrix} b\sin\theta \\ 2U \int dx_2 \\ 0 \end{pmatrix} + \begin{pmatrix} b\cos\theta & b\cos\theta \\ - \int (-\sigma_y) \frac{\partial u_1}{\partial x_1} dx_1 - & \int \sigma_y \frac{\partial u_2}{\partial x_1} dx_1 \\ 0 & 0 \end{pmatrix} \quad (28)$$

$$= \underbrace{2Ub\sin\theta}_{\text{Avg SERR due to shearing}} + \underbrace{\sigma_Y \left[\int_0^{b\cos\theta} \frac{\partial(u_1 - u_2)}{\partial x_1} dx_1 \right]}_{\text{Yield hoop stress X Radial CTOD}} \quad (29)$$

From the above expression it is clear that during the rebar pullout, circumferential cracking near upper unconfined surface takes place resulting in the formation of a conical plug. The expression also confirms the presence of the average shearing component which contributes to the slip over the projected length of the conical geometry. According to NBS studies, cracking initiated at the upper edge of the disc results due to 30 to 40 percent of the ultimate load and ends the elastic response. The circumferential crack grows towards the reaction ring until it's inhibited by aggregate interlock. This cracking system which appears to be stable is termed as primary cracking.

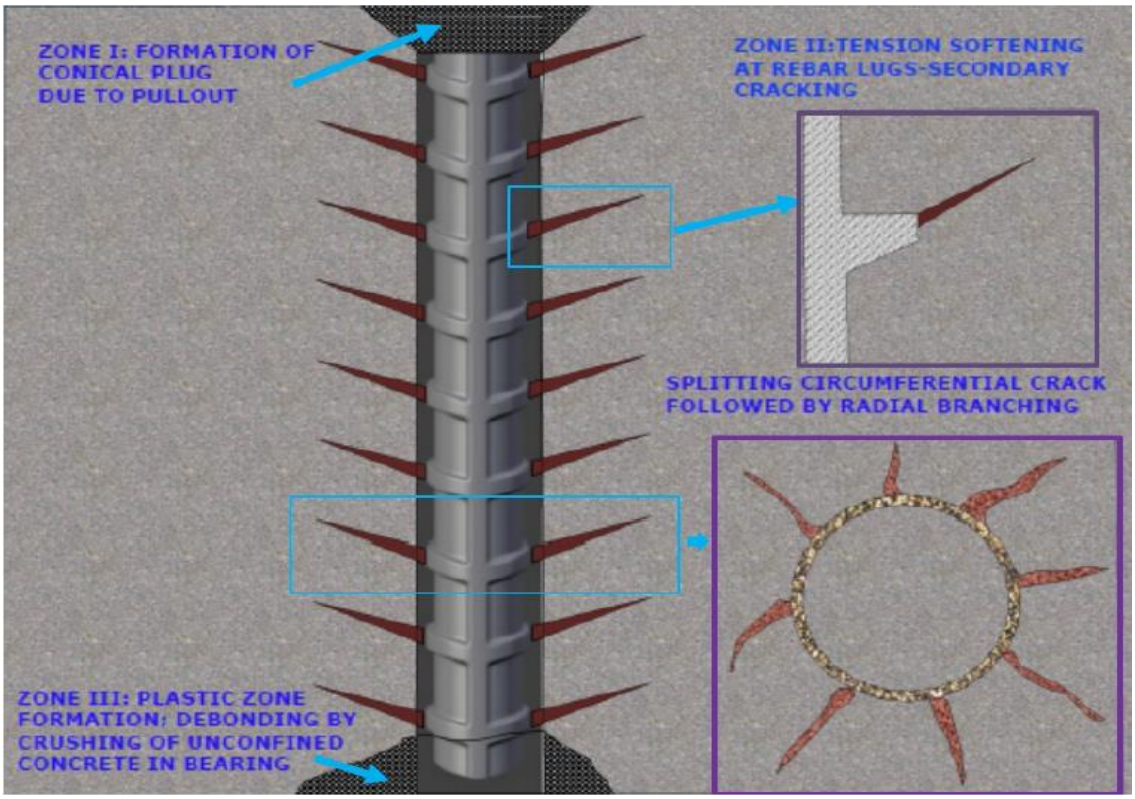

Fig 12. EPFM model of rebar specimen subjected to pullout forces subdivided into failure zones

The Zone II region consists of microcracks originating out of the lugs in reinforcement that branch out at angles between 25 to 45 degrees, resulting in secondary fracture running from upper edge of disc to inside edge of the support ring. Large tensile strains perpendicular to the microcracks exist at the tip of the splitting zone (the outer edge ring formed by multiple coalescing microcracks) and tend to decrease rapidly towards the reaction ring, before initiation of the circumferential cracks. However, during this growth process, the radial direction experiences large tensile stresses. The splitting failure caused by wedging action of lugs produces confined compressive stresses on the surrounding concrete, balanced by the hoop stresses around the bar. This radial splitting causes catastrophic debonding of the rebar.

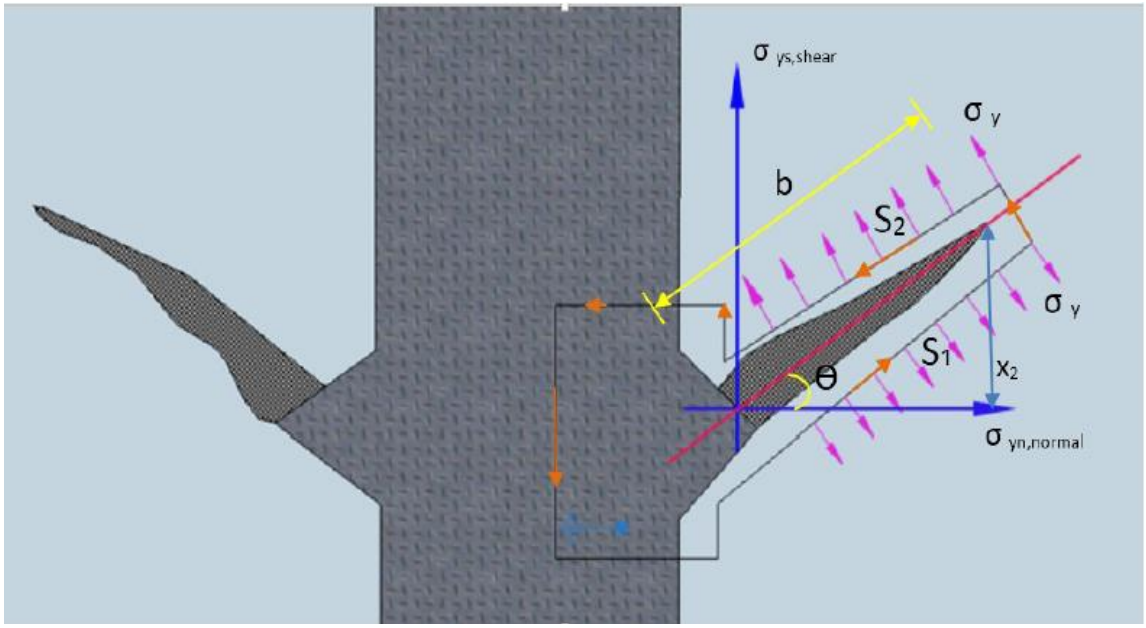

Fig 13.Magnified image of contour surrounding tension softening zone around crack originating from shear lug

The microcracks originating from the lugs can be modelled using a tension softening model quite similar to pullout of studs. The J value for the lug can be obtained as

$$J_{lug} = \left(\int_{\Gamma_{steel}} \sigma(\delta) d\delta_1 + \int_{\Gamma_{concrete}} \sigma(\delta) d\delta_2 \right) - \underbrace{\int_{\Gamma_{lug}} T^{lug} \cos\theta \frac{\partial u^{lug}}{\partial x} dS_{pz}}_{circumferential\ traction\ component} - \underbrace{\int_{\Gamma_{lug}} T^{lug} \sin\theta \frac{\partial u^{lug}}{\partial x} dS_{pz}}_{shearing\ traction\ component} + \frac{K_{tip}^2 (1-\nu^2)}{E} \tag{30}$$

where δ_1 and δ_2 are smeared crack displacements and θ is angle of the crack to the horizontal plane. K is a softening function which relates the crack tip opening at a distance *r* from the axis of rotation to the circumferential stress σ(θ) and critical cracking strain ε_θ^c [28] as

$$\varepsilon_\theta^c = n^c \frac{w(r)}{2\pi r} \Rightarrow \sigma_\theta = f[w(r)] = f\left(\frac{2\pi r}{n_c} \varepsilon_\theta^c \right) = K_{tip} \tag{31}$$

where $w(r)\rightarrow$ opening of each crack at distance r from axis of rotation, and $n_c\rightarrow$ number of cracks.

Zone III represents a plastic zone formation due to crushing of surrounding confined concrete. This stage is a consequence of the fracture growth and propagation in Zone II III, and does not contribute to the slip primarily or secondarily.

Tepfers et al.[29] performed a simplified analysis of splitting cracks resulting from the circumferential or normal stress(σ) and related it to the interfacial shear stress(τ) and postulate a Coulomb-type failure criterion as

$$\sigma = \tau \tan\phi \tag{32}$$

ϕ is the constant complimentary friction angle valid for pseudo-static cases. This was then modified by Rosati et al.[30] taking cohesion into consideration as

$$\sigma = (\tau - \tau_o) \tan\phi \tag{33}$$

3.5. Constitutive elasto-plastic modelling for pseudo-static SSI

Micromechanical behavior at the granular media-structure interface is of major concern as far as design of shallow and deep foundations, retaining structures, sheet piles, earth reinforcements and other geotechnical structures are considered. The frictional characteristics, failure planes and cohesion of soil have been studied through various experimental, theoretical and constitutive models. The use of thin layered interface elements had been proposed by Desai et al.[31], which is treated as a solid finite element with its incremental stress-strain components linked by a constitutive stiffness matrix consisting of normal and shear components as well as coupling effects. A variety of tests, have been used to model the soil-structure interface. Fakharian[32] and Tejchman et

al.[33] performed modified direct and simple shear tests on sand steel interfaces to study shear zone thicknesses and friction angles, when subjected to varied boundary conditions under constant 2D and 3D normal stresses. Similar experiments were performed using advanced imaging techniques[34] to account for failure modes during interface shearing and sand particle deformation to understand strain hardening/softening and dilatancy effects. Desai et al.[35] performed cyclic loading tests using CYMDOF(cyclic multi degree of freedom device) which allowed for translational, normal and rotational motions under direct and simple shear deformations for both drained and undrained laws.

Similarly, a large number of non-linear elastic, elasto-plastic, visco-elastic and directional-type models have been proposed to model strength parameters and stress-displacement relations which affect the load deformation behavior. Most of these models use Mohr-Coulomb yield functions with incremental constitutive equations to define empirical material parameters governing the displacements and stress distributions at soil-structure interface. However, these empirical models cannot be generalized for all types of soil media, which, being a multi-phase material depends greatly on interface roughness, moisture content, particle size distribution. The different phases of soil-structure interfaces when subjected to monotonic shearing and constant normal stresses can be subdivided into: (i) intact phase: LEFM concepts can be applied during this stage. During this phase the interface crack can be treated as a Griffith crack subjected to far field stresses which can help us obtain asymptotic stress fields at the crack tip and fracture toughness parameters. (ii) The critical phase (when the soil sample reaches it’s maximum dilation or compressive state): The critical state is when the loose particles interlock themselves in a state under which tangential displacement ceases to increase

with increasing shear stress. When the interface is subjected to cyclic loading the local initial densities, initial confinement stresses and number of loading cycles also play a crucial role. Fracture propagation can be monitored using Dugdale type elasto-plastic model with a strain hardening/softening function depending on smoothening or roughening of interface. When subjected to cyclic loading the non-linear loading-unloading reloading response can be simulated using a modified Ramberg-Osgood model [30] (iii) the disturbed phase: During this phase shear stresses ceases to increase with increase in shear displacement due to interlocking of granular particles.

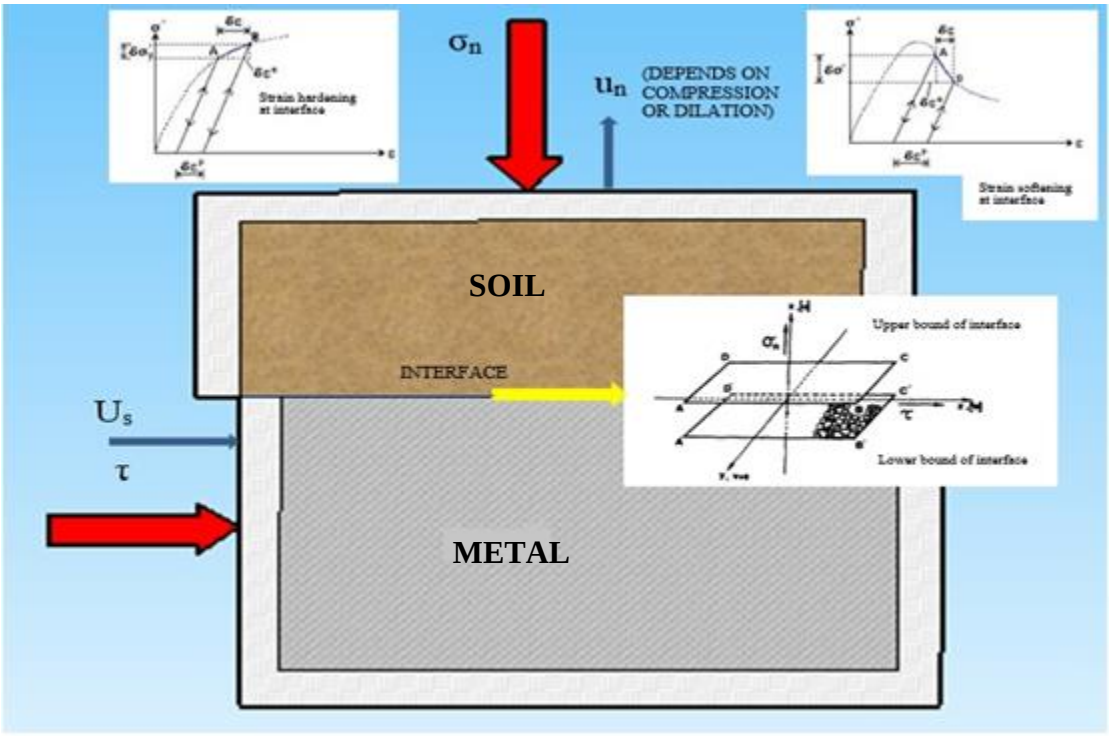

Fig 14: Modified direct shear tests with interface parameters and strain hardening/softening effects during critical phase

However the cohesion and friction angle are bound to change if the constant normal applied stress changes. The fracture state can be assumed to be purely plastic.

The proposed analytical model can be used for qualitative assessment of crack propagation and impinging effects of modified direct shear tests that do not pre-define the failure plane for granular media-structural interfaces, which is a scope of future studies.

CHAPTER 4. COMPUTATIONAL IMPLEMENTATION

The efficiency of computational methods for verification of the proposed analytical model depends on the effective implementation of displacement discontinuities that do not conform to inter-element surfaces. The proposed approach (as discussed in Chap. 2) uses the conservation of energy principle for evaluation of crack initiation and growth in a controlled volume. A similar energetic approach, the eXtended Finite Element Method (XFEM) is adopted for modelling growth of a predefined crack front to analyze the strain energy release rate (SERR) and stress intensity factors (SIF) assuming multiple contours around the crack tip. XFEM uses the partition of unity approach to model strong and weak discontinuities in a mesh-independent framework. This facilitates implementation of discontinuous functions into a conventional finite element scheme by use of additional degrees of freedom and enrichment functions [36, 37]

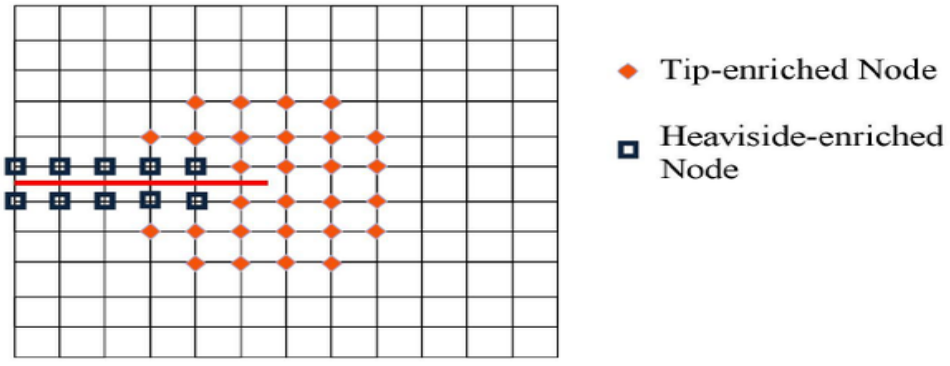

Fig 15: Crack front propagation using enriched Heaviside function in XFEM

The enrichment functions are shifted such that they vanish at the nodes, since the nodal displacement is a function of both the established and enriched DOF. Cracks are modeled using a combination of two enrichment functions; one for the stress concentration at the crack tip and a Heaviside step function to represent the discontinuity across the body of the crack [38]. The Heaviside function accepts a value of 1 above the crack face and -1 below the crack, thus inserting a displacement discontinuity across the crack domain in elements whose local support is cut by the crack.

$$\upsilon_{\alpha}(x)_{,\alpha=1-4} = \left[\sqrt{r}\sin\frac{\theta}{2}, \sqrt{r}\cos\frac{\theta}{2}, \sqrt{r}\sin\theta\sin\frac{\theta}{2}, \sqrt{r}\sin\theta\cos\frac{\theta}{2}\right] \tag{34}$$

where, r and Θ are polar coordinates with origin at the crack tip and its principal axis parallel to the crack face.

For the crack tip the enrichment functions shown above, were originally introduced in the element-free Galerkin method [39] and later adopted for use in XFEM [38]. These four functions span the crack tip displacement field. Upon solving the system of equations, the enriched DOF's can be used for interpolating within a particular element. The enriched elements are able to handle strain discontinuities, significantly reducing the pre-processing time that may arise due interface-mesh misalignment.

A model's response contains large amount of tabulated data pertaining to its strain, stress and displacement which is difficult to grasp as whole. Stress intensity factors help in condensing the data, considerably reducing the complexity and post-processing analysis time. The domain form of the contour interaction integral is used in the present study to compute SIF's along a static crack for steel-concrete and concrete-concrete

interface. The interaction integral involves superposition of auxiliary fields onto the actual fields produced by the solution of a BVP.

4.1 ABAQUS implementation

ABAQUS [40] supports contour integral evaluations for an arbitrary stationary surface crack without the need to conform the mesh to the geometry of the discontinuities. Furthermore, only 1st order brick and 1^{st} and 2^{nd} order tetrahedron elements with isotropic elastic material configuration can be used for modelling stationary cracks. This limits the scope of setting up benchmark models for validation of the analytical model. However efforts have been made to set up individual models for analysis of SIF using static cracks. The finite element model treats each contour as a ring of elements surrounding the crack tip from one face to another, defined recursively to surround previous contours [40]. Crack propagation across an interface is studied for a plane strain block subjected to tensile forces using the cohesive segments approach, based on the theory that substantial cohesive molecular forces exist near the crack-tip where two crack surfaces are in close vicinity.

Intensity of the forces attain a maximum value when tensile strength of the material is reached and starts to decrease as the crack faces start opening up. The region between the point where the normal stress equals the tensile strength and the point at which the crack opening displacement is equal to the critical opening, is called the cohesive zone [41]. ABAQUS employs phantom nodes and cohesive segments for ductile/brittle fracture governed by pressure overclosure relationship when crack is closed and cohesive behavior contributes to normal contact stresses when crack is open. When simulating XFEM cracks, it is essential to specify damage initiation criterion in the

material property definition. The maximum principal stress (MAXPS) criterion is adopted for the benchmark models used in the current study.

Crack initiation also depends on the stress/strain concentrations in enriched nodes and occurs when the max principal stress reaches a critical value (q=1) where $q = <\sigma_n>/\sigma^0_{max}$. The crack plane is perpendicular to the max principal stress and is capable of handling a changed crack plane or direction of propagation. A damage evolution criterion for traction separation law based on energy or displacement was used in conjunction with the initiation criterion. As the crack grows along an interface, the structural response is rendered non-linear or non-smooth making it difficult to attain convergence. Furthermore, the crack feature in ABAQUS is limited to implicit analysis. Therefore, viscous regularization was activated for convergence with the Newton method. The stabilization value was chosen such that the response is unaffected while attaining convergence.

The major limitation associated with XFEM application to bimaterial interfacial cracks, is associated with the crack definition itself. The assembly of a crack at the junction of two independent material domains is not allowed. Hence, a single domain was partitioned and the corresponding material properties were assigned to each partition. The principal attraction of meshfree methods is their capacity to deal with moving boundaries and discontinuities such as phase changes and crack propagation. Hence, the XFEM_CRACK_ GROWTH interaction feature was used to analyze impinging characteristics of a progressing crack front. This feature was switched off for evaluation of stress intensity factors.

For crack tip visualization, stress field contours were requested for mode-II loading of the uncracked domain. The output variables requested for crack tip simulation

of rectangular bi-material plate with an interfacial crack (will be discussed in next section) are as follows:

- PHILSM: Signed distance function describing crack surface
- PSILSM: Signed distance function describing the initial crack front.
- ENRRTXFEM: SERR components when XFEM is used for LEFM.
- STATUSXFEM: Status of Heaviside enriched element. (1.0 if the element is completely cracked and 0.0 if the element contains no crack)

4.2. Results and discussions

A bimaterial plate with considerable thickness (plane stress) for uni- (concrete-concrete) and bi-material (concrete-steel) interfacial crack with a static crack front was simulated in a single step for evaluation of SIF's using the domain contour integral approach. A similar model with smaller thickness (plane strain) was adopted for computing the SERR for a growing crack. The variations in crack path and Strain Energy Release Rate interfacial cracks are observed for varied loading intensities.

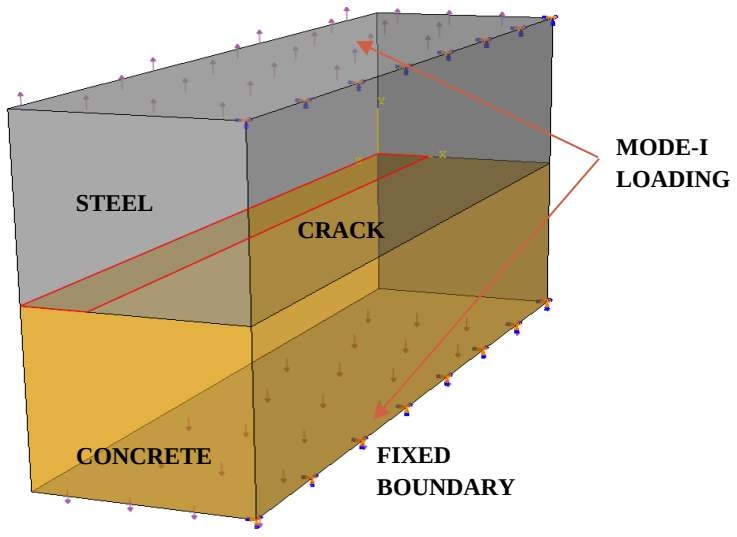

Fig 16: Undeformed FE model for the steel-concrete interface

4.2.1. Analysis of stress/displacement fields and computation of SIF

A domain size of 4000 mm X 2000 mm X 1000 mm was assumed for the simulations with an initial crack tip of 300 mm. The model is fixed at the edges with uniform pressure applied on the top and bottom surface to simulate opening mode loading. A structured mesh with reduced integration 8-noded linear brick elements (C3D8R) with hourglass control was adopted for the model. The stress intensity factors were computed on the basis of max energy release initiation criterion. It is important to note that the crack propagation and node enrichment is stopped; as contour integral evaluation is possible only for a static crack front. Parametric studies performed on the specimen reveal that for an increase in the CTOD, the K_I (mode-1 SIF) increases while K_{II} (mode-2 SIF) decreases. Similar trends were observed for both concrete-concrete and concrete-steel interfaces. The stress fields are observed to be symmetric for uni-material interfaces while the bi-material cracks show some distortion primarily due to elastic moduli mismatch.

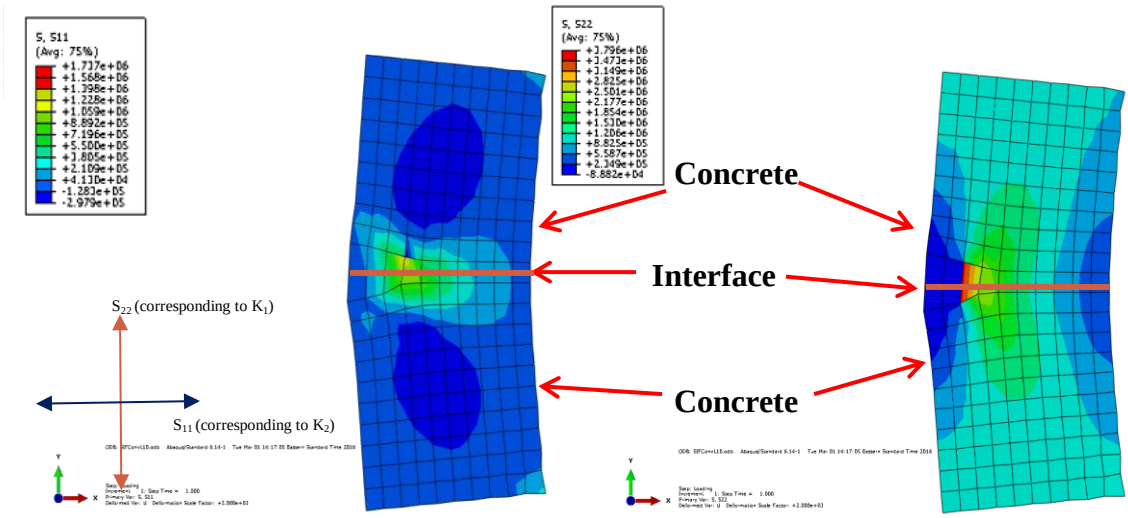

Fig 17: Stress field contours, S_{11} and S_{22} for static crack across concrete-concrete interface

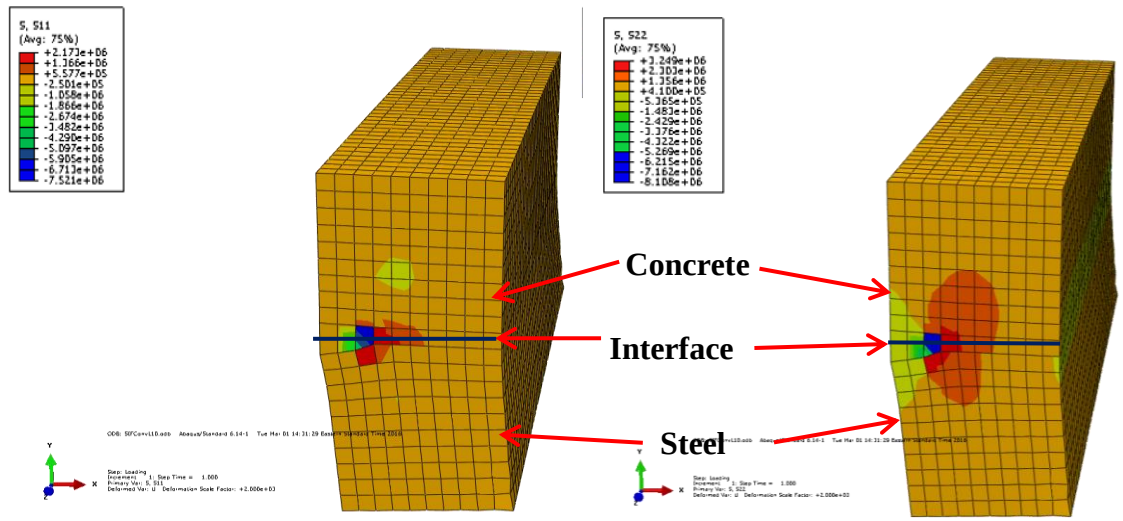

Fig 18: Stress field contours, S_{11} and S_{22} for static crack across steel-concrete interface.

From the results presented in Fig. 17 and 18; it is observed that there is continuity in the stress field with small discontinuities in the case of bimaterial interface. Also, higher stress concentrations are observed at the concrete part of the bi-material interface. The displacement field for unimaterial interface is symmetric; while it is considerably large for the concrete in the bimaterial model as shown in Fig. 19.

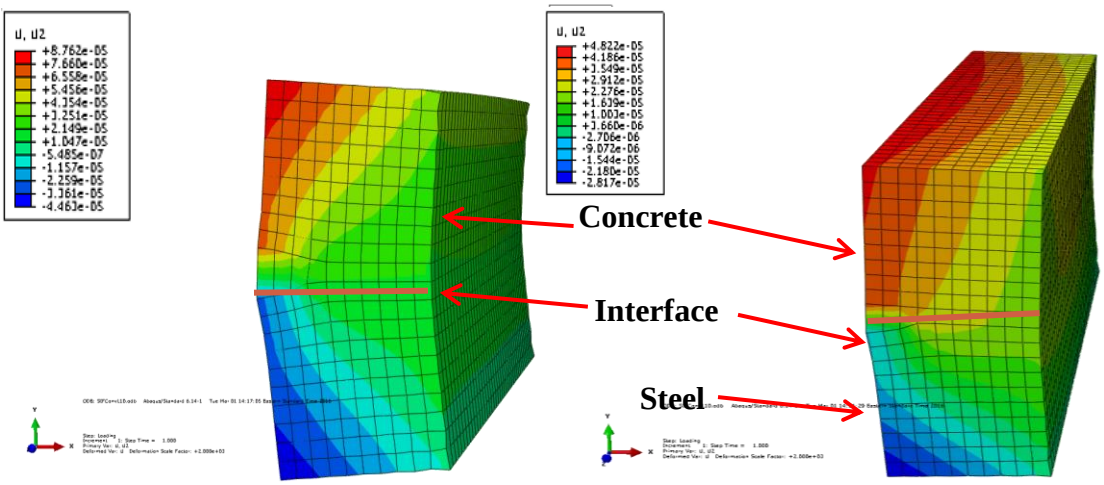

(a) (b)

Fig 19: Displacement field contours, U_2 for (a) concrete-concrete interface and (b) steel-concrete interface

The simulation results presented in Table 1 and 2, which gives the stress intensity factors (K_1, K_2 and K_3) and J estimates of three contours enclosing the crack tip for six time increments of crack propagation along crack front propagation direction (MERR=0 deg). It is observed that the normalized values of K_I increases while K_{II} decreases with the increase of elastic modulus ratio, which are in agreement with the literature [42, 43]. Parametric studies also indicate that both K_1 and K_2 decrease with the increase in crack tip opening. The analytical model highlights the fact that the J-Integral is a close measure of the fracture energy of the cracked domain. Upon extending this idea to the XFEM model for concrete-concrete interface; the fracture energy values were found to be quite similar to those in literature derived empirically and from traction softening laws (ref. Table 3). Furthermore, the J estimates for individual contours yielded nearly equivalent data enforcing the path independent property. The J for the crack propagating along steel concrete interface is considerably larger (around twice) than concrete-concrete interface; which can be associated with plastic zone formation and evolution of residual energy.

Table 1: Stress Intensity (K) Factor estimates of contour integrals (n=3) for concrete-concrete interfacial crack

K F A C T O R E S T I M A T E S

CRACK NAME	CRACKFRONT NODE SET		CONTOURS 1	2	3
EDGECRACK					
	XFEM_1	K1:	2.1446E+06	1.6574E+06	1.7027E+06
		K2:	-2.8091E+04	-1.1381E+04	2.5717E+04
		K3:	7.0596E+04	1.4320E+05	1.4111E+05
	MERR	DIRECTION (DEG):	0.000	0.000	0.000
		J from Ks:	147.4	88.74	93.60
	XFEM_2	K1:	2.1206E+06	1.5893E+06	1.6423E+06
		K2:	-1.5860E+04	-1.3241E+04	1.4727E+04
		K3:	1050.	3.1292E+04	1.8895E+04
	MERR	DIRECTION (DEG):	0.000	0.000	0.000
		J from Ks:	143.9	80.86	86.32
	XFEM_3	K1:	2.1491E+06	1.6442E+06	1.6897E+06
		K2:	-1.4350E+04	-6421.	3.2237E+04
		K3:	-8186.	-4821.	-3385.
	MERR	DIRECTION (DEG):	0.000	0.000	-1.152
		J from Ks:	147.8	86.50	91.38
	XFEM_4	K1:	2.1588E+06	1.6477E+06	1.6964E+06
		K2:	-1.6334E+04	-1.0144E+04	1.8691E+04
		K3:	-2224.	5494.	1153.
	MERR	DIRECTION (DEG):	0.000	0.000	0.000
		J from Ks:	149.1	86.87	92.09
	XFEM_5	K1:	2.1638E+06	1.6546E+06	1.7003E+06
		K2:	-1.5323E+04	-1.0774E+04	2.4778E+04
		K3:	-1926.	3753.	1249.
	MERR	DIRECTION (DEG):	0.000	0.000	0.000
		J from Ks:	149.8	87.60	92.52
	XFEM_6	K1:	2.1669E+06	1.6551E+06	1.7028E+06
		K2:	-1.6790E+04	-8230.	2.1608E+04
		K3:	-854.4	1667.	358.1
	MERR	DIRECTION (DEG):	0.000	0.000	0.000
		J from Ks:	150.2	87.64	92.79

Table 2: Stress Intensity (K) Factor estimates of contour integrals (n=3) for steel-concrete interfacial crack

K F A C T O R E S T I M A T E S

CRACK NAME	CRACKFRONT NODE SET		C O N T O U R S 1	2	3
EDGECRACK					
	XFEM_1	K1:	8.7003E+06	6.7921E+06	6.9249E+06
		K2:	-1.6442E+05	5.0808E+05	7.2692E+05
		K3:	-1.1556E+06	-1.9845E+06	-2.5105E+06
	MERR	DIRECTION (DEG):	1.008	-8.676	-11.63
		J from Ks:	353.2	236.7	261.6
	XFEM_2	K1:	8.4338E+06	6.4227E+06	6.5615E+06
		K2:	-1.1372E+05	6.1766E+05	8.5581E+05
		K3:	-4.4321E+05	-4.1833E+05	-5.0113E+05
	MERR	DIRECTION (DEG):	0.000	-10.73	-14.33
		J from Ks:	325.0	190.6	200.9
	XFEM_3	K1:	8.4392E+06	6.5864E+06	6.6580E+06
		K2:	-8.7557E+04	6.6965E+05	8.9403E+05
		K3:	-3.4968E+05	-3.0236E+05	-3.3611E+05
	MERR	DIRECTION (DEG):	0.000	-11.27	-14.76
		J from Ks:	324.9	200.0	206.1
	XFEM_4	K1:	8.4361E+06	6.5828E+06	6.6484E+06
		K2:	-4.7620E+04	7.0727E+05	9.4392E+05
		K3:	-2.8728E+05	-2.3991E+05	-2.5893E+05
	MERR	DIRECTION (DEG):	0.000	-11.88	-15.62
		J from Ks:	324.4	199.8	205.6
	XFEM_5	K1:	8.4335E+06	6.5825E+06	6.6377E+06
		K2:	-7219.	7.3895E+05	9.8396E+05
		K3:	-2.4640E+05	-2.0966E+05	-2.1701E+05
	MERR	DIRECTION (DEG):	0.000	-12.38	-16.31
		J from Ks:	324.0	199.9	205.2
	XFEM_6	K1:	8.4305E+06	6.5765E+06	6.6327E+06
		K2:	2.3315E+04	7.6488E+05	1.0141E+06
		K3:	-2.1430E+05	-1.8419E+05	-1.8913E+05
	MERR	DIRECTION (DEG):	0.000	-12.82	-16.81
		J from Ks:	323.7	199.7	205.1

Table 3: Comparison of computed fracture energy with existing model for concrete

Reference	Computation results from XFEM (N/mm)	Model	Fracture energy (N/mm)
Gustaffson & Hillerborg [44]	0.148 ± 0.0015 (concrete-concrete interface)	Bilinear softening	0.140
Guinea et al. [45]		Bilinear softening	0.145
Reinhardt [46]		Power relation	0.083 - 0.142
CEB-FIP model [47]		Empirical	0.0825 ± 0.025
Bazant and Becq-Giraudon [48]		Empirical	0.112 ± 0.034
NA	0.323 ± 0.002 (steel-concrete interface)		

** Fracture energy for steel-concrete interface has not been validated due to lack of data in literature (as per author's knowledge)*

4.2.2. Crack growth characteristics and computation of Strain Energy Release Rate

The determination of crack path is performed by predicting the direction and magnitude of crack front at each iteration. ABAQUS avoids consideration of near-tip asymptotic stress singularity by propagating the crack across an entire element at a time. The cohesive damage modeling approach with traction separation parameters is considered for the current model. An uncracked domain of 100 mm X 50 mm X 2 mm is used for all crack growth models. The domain is subjected to mode 2 loading and constrained to move along the direction of loading. The applied pressure is ramped up till the principal failure stress is reached, and continued until the domain is completely penetrated by the progressing crack front.

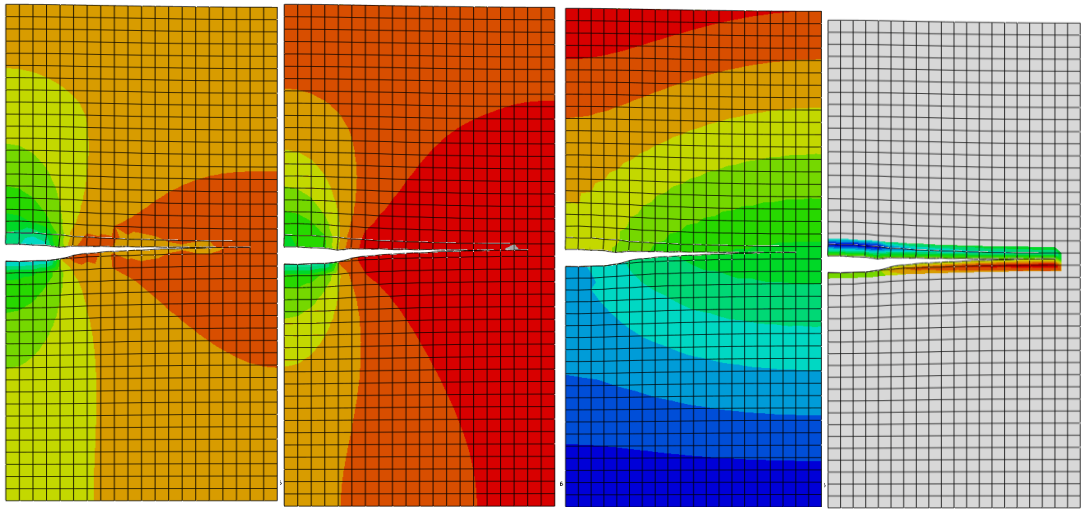

(a) (b) (c) (d)

Fig 20: (a) S_{11} (b) S_{22} (c) U_2 (d) PHILSM for crack propagating along concrete-concrete interface

The stress (see Fig 19 a and b) and displacement contours (see Fig 19 c) are symmetric when the crack propagates along unimaterial interface. Also, the opening of nodes above and below the cracks occurs for the same time increment. However, as expected, the crack seems to impinge from the interface towards the concrete domain for the bimaterial

(as observed in Fig 20), which occurs due to variations in the normal threshold stresses and moduli mismatch. The contours also indicate higher stress localization along the concrete edge of the crack front)

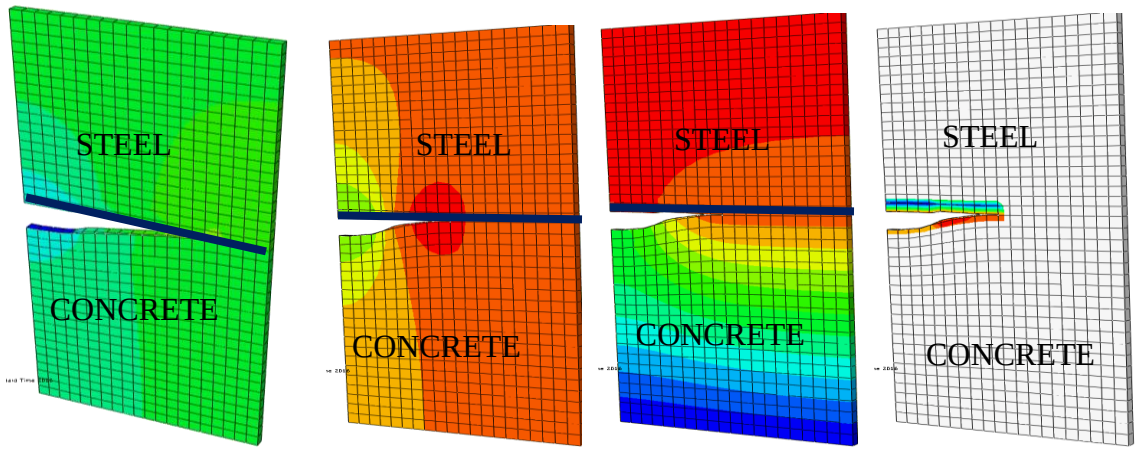

Fig 21: (a) S_{11} (b) S_{22} (c) U_2 (d) PHILSM for crack propagating along steel-concrete interface

The Strain Energy Release is computed over the simulation period and is observed to spike up once the threshold normal stress is attained. Furthermore, the rate of energy release significantly increases as the mode 1 loading is proportionally increased.

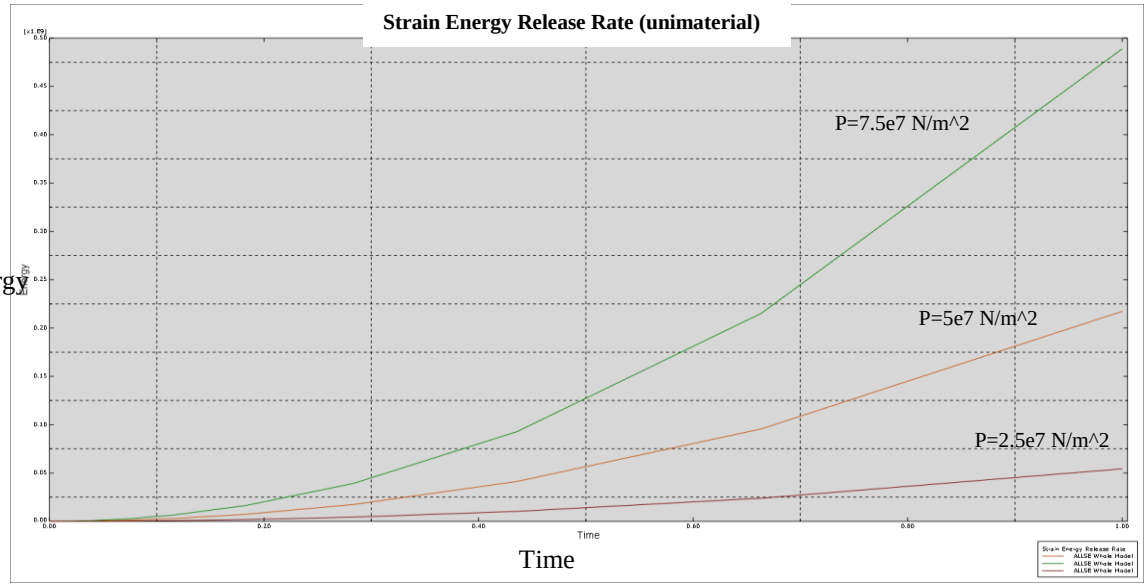

Fig 22: SERR for unimaterial interface crack under opening mode loading

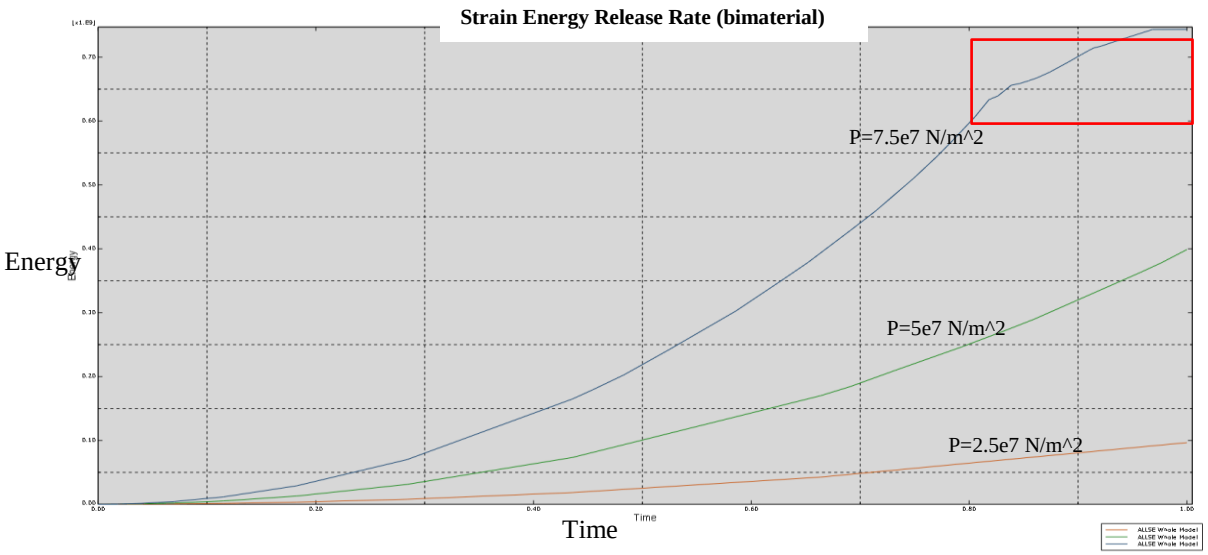

Fig 23: SERR for bimaterial interface crack under opening mode loading

For the steel-concrete interface crack, the strain energy release rate is observed to subside when the loading is spiked up. Such behavior can be associated with the evolution of residual energy arising due to elastic moduli mismatch across the interface. The CTOD also sharply decreases at this point even when the loading increases (see Fig. 23). The first short plateau (circled in blue) can be attributed to the crack initiation followed by unloading process when the crack tip opening starts decreasing.

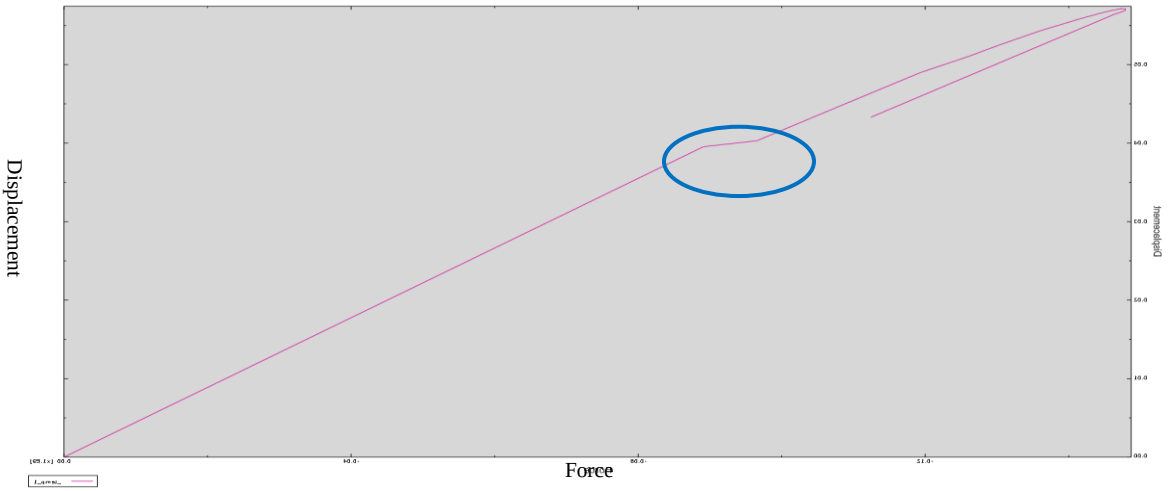

Fig 24: F vs CTOD for bimaterial interface crack under opening mode loading (P= 7.5e7 N/mm^2)

CHAPTER 5. CONCLUSIONS

A comprehensive energy-based approach was developed in the thesis to assess the fracture toughness parameters pertaining to the fundamental failure modes of bimaterial interfaces. The controlled volume fracture model was used (in Chap. 2) to correlate the fracture energy released during crack growth to the potential energy of the entire system. Using the conservation of energy principle, a suitable stress strain relation was derived in terms of the strain energy released, which can be obtained from experimental data and therefore allow us to calibrate the model. The potential energy release rate was obtained for a contour surrounding the crack tip in terms of the strain energy release rate and traction slip parameters. The J-integral was used to compute the strain energy release rate and crack tip opening displacement. Path independence of the J-integral provides the freedom to frame the boundary value problem for a domain where the stresses and tractions are well defined. This allows us to bypass the numerical complexities associated with computation of asymptotic stress fields. After some numerical analysis, The J-integral was found to be the difference between the gross strain energy release rate (SERR) and the tangential traction slip energy for bimaterial interface.

For a growing crack, the paradox is that when strains and stresses are singular but their singularity is not strong enough to obtain a non-zero local energy release rate,

there is no energy surplus for crack production [49]. The model attributes the surplus energy to plastic dissipation with probable strain hardening/softening. Plasticity effects at the crack tip were addressed by adopting a boundary interface path surrounding the crack tip assuming crack front yielding. The J-integral was linked to the crack tip opening (CTOD); since evaluation of strain energy rate was not possible for an equivalent elastic crack field corresponds to the 'deformation theory of plasticity'. For small plastic deformations, J was expressed as the product of the crack tip opening displacement (CTOD) and the yield stress at the crack tip (σ_Y) (see Sec 2.3).

The analytical model presented in Chap. 2 was applied to some common bimaterial interfaces (the stud-microstructure-steel plate and rebar-concrete interface). A crack front was assumed for each case depending on test data available in literature and the contour integral paths were defined for each case such that individual material properties and loading parameters can be used to formulate the problem statement. Appropriate tension softening effects associated with the crack tip progression were implemented using a correction term. The fracture toughness and stress intensity factors were evaluated empirically. The different stages of microstructural failure of the rebar concrete interface were analyzed. The strain energy values (in terms of J) can help us in assessing the governing failure mode and provide valuable information about the damage expansion phenomenon from micro to macro scale for structural elements. There is some practical significance attached to the energy conservation approach, as it helps develop an understanding of deterministic parameters irrespective of crack-tip singularities and applied loading. The level of external loading responsible for imparting instability to a pre-existent crack is difficult to obtain. Using XFEM techniques, the

contour integrals were evaluated at each node of the crack front (ref Chap.4). The interfacial fracture energy of uni-material (concrete-concrete) interface was computed from a XFEM static crack model. The results were in close agreement (variation of 10%-15%) with existing analytical and empirical models in literature. Fracture energy computed for the bimaterial (steel-concrete) interface was found to be twice that of concrete-concrete interface (could not be verified due to lack of experimental data). The SIF values were found to converge for individual contours conforming to the path independence property. For a growing crack, the strain energy release rate was observed to significantly increase with the increment of mode-1 loading applied on the domain. The rate of increase for bimaterial interface was observed to be steeper than the unimaterial interface as the loading was ramped up. As expected from the numerical computation (ref. Sec 2.3), the model also showed impinging of the crack towards concrete, due to lower elastic modulus.

Even though conformal meshing is not essential for modelling a discontinuity using XFEM, it is difficult to achieve a good convergence rate and high accuracy for problems with moving domain. Computational difficulties from domain dependence arising due to variations in the approximate finite element solutions require continuous mesh refinement. The model proposed is not suitable for cracks propagating at high strain rates. Also, material discontinuities and incremental plasticities have not been accounted for. The scaling of the model for macroscopic failure response of the structure in accordance with size effect laws is a topic of future studies. However, with the use of appropriate strain hardening/softening function, this model can be applied to a variety of

ductile-brittle interfaces with largely varying Young's modulus, resulting in close formed solutions for the strain energy release rate and crack tip opening displacements

BIBLIOGRAPHY

BIBLIOGRAPHY

[1]Rice, J. (1968). A Path Independent Integral and the Approximate Analysis of Strain Concentration by Notches and Cracks. Journal of Applied Mechanics, 35(2), 379.

[2] Rybicki, E.F., & Kanninen, M.F. (1977). A finite element calculation of stress intensity factors by a modified crack closure integral. *Engineering Fracture Mechanics, 9*(4), 931-938.

[3] Darling, K., & U.S. Army Research Laboratory. (2011). *Thermally stable nanometals by predictive atomic scale interfacial energy reduction* (ARL-TR (Aberdeen Proving Ground, Md.) ; 5490). Aberdeen Proving Ground, Md.: Army Research Laboratory.

[4] Tuakta, C., & Büyüköztürk, O. (2011). Deterioration of FRP/concrete bond system under variable moisture conditions quantified by fracture mechanics. *Composites Part B: Engineering*, *42*(2), 145-154.

[5]A.G. Evans, M. Rühle, B.J. Dalgleish, P.G. Charalambides, "The fracture energy of bimaterial interfaces", Materials Science and Engineering: A, Volume 126, Issues 1–2, 15 June 1990, Pages 53-64

[6] M. L. Williams, "The stresses around a fault or crack in dissimilar media" *Bulletin of the Seismological Society of America* (April 1959), 49(2):199-204

[7] Sih, G., & Rice, J. (1964). The Bending of Plates of Dissimilar Materials With Cracks.*Journal of Applied Mechanics, 31*(3), 477.

[8] Rice, J., & Sih, G. (1965). Plane Problems of Cracks in Dissimilar Media. *Journal ofApplied Mechanics, 32*(2), 418.

[9] Rice, J. (1988). Elastic Fracture Mechanics Concepts for Interfacial Cracks. *Journal of Applied Mechanics, 55*(1), 98.

[10]Buyukozturk, Oral, Lee, Kwang-Myong. (1993)."Assessment of interfacial fracture toughness in concrete composites". Cement and Concrete Composites, 15(3), 143-151.

[11]Dundurs, J. (1969). Discussion: "Edge-Bonded Dissimilar Orthogonal Elastic Wedges Under Normal and Shear Loading" (Bogy, D. B., 1968, ASME J. Appl. Mech., 35, pp. 460–466). Journal of Applied Mechanics, 36(3), 650.

[12]Buyukozturk, Oral, Hearing, Brian. (1998)."Crack propagation in concrete composites influenced by interface fracture parameters". International Journal of Solids and Structures, 35(31), 4055-4066.

[13]Bruhwiler, E., Wittmann, F.H. (1990). "The wedge splitting test, a new method of performing stable fracture mechanics tests". Engineering Fracture Mechanics, 35(1), 117-125.

[14]Walter, Rasmus, Ostergaard, Lennart, Olesen, John F., Stang, Henrik. (2005). "Wedge splitting test for a steel–concrete interface". Engineering Fracture Mechanics, 72(17), 2565-2583.

[15] RILEM TC-108. Interfacial transition zone in concrete. RILEM Report 11. Chapman and Hall, 1996.

[16] P.Ponte Castañeda, P.A. Mataga, Stable crack growth along a brittle/ductile interface—I. Near-tip fields, International Journal of Solids and Structures, Volume 27, Issue 1, 1991:105-133

[17] Bose, K. Ponte, P. Ponte Castañeda, and P. Ponte Mataga. "Stable Crack Growth along a Brittle Ductile Interface - II. Small Scale Yielding Solutions and Interfacial Toughness Predictions." *International Journal of Solids and Structures* 36.1 (1999): 1-34.

[18] Soh, C., Chiew, S., Dong, Y. (1999). "Damage Model for Concrete-Steel Interface". Journal of Engineering Mechanics, 125(8), 979-983.

[19] Hutchinson, J. (1968). Singular behaviour at the end of a tensile crack in a hardening material. *Journal of the Mechanics and Physics of Solids, 16*(1), 13-31.

[20] Dugdale, D. (1960). "Yielding of steel sheets containing slits". Journal of the Mechanics and Physics of Solids, 8(2), 100-104.

[21] Yuan, Huang, & Brocks, Wolfgang. (1991). On the J-integral concept for elastic-plastic crack extension. *Nuclear Engineering and Design, 131*(2), 157-173.

[22] Shan-suo, Li Lei, Wang Bin.(2009)"Shear transmitting capacity of interface between steel and concrete".Engineering Mechanics.Vol. 26, No.3,p.148

[23]Li, Victor C. (1997). "Applicability of J-integral to tension-softening materials". Journal of Engineering Mechanics, 123(5), 531.

[24] Ballarini, R., Shah, S., & Keer, L. (1986). Failure Characteristics of Short Anchor Bolts Embedded in a Brittle Material. *Proceedings of the Royal Society of London. Series A, Mathematical and Physical Sciences, 404*(1826), 35-54.

[25]Bazant, Zdenek P., Vitek, Jan L. (1999). "Compound size effect in composite beams with softening connectors".(part one: energy approach). Journal of Engineering Mechanics, 125(11), 1308.

[26] ACI 318-14: Building code requirements for Structural concrete

[27]Ingraffea, A.R., Gerstle, W.H., Gergely, P., Saouma, V. (1984). Fracture mechanics of bond in reinforced concrete: J. Struct. Division ASCE, Vol 110 No 4 (April 1984). Computer-Aided Design, 16(6), 339

[28]Bazant, Z., Planas, J. (1998). Fracture and size effect in concrete and other quasibrittle materials (New directions in civil engineering). Boca Raton: CRC Press.

[29]Tepfers, R., Chalmers Tekniska Hgskola. (1973)."A Theory of Bond Applied to Overlapped Tensile Reinforcement Splices for Deformed Bars."

[30]Rosati, Modeling of Local Bar-to-Concrete Bond in RC ... to Practice, CEB-RTU, Vol. 3, pg. 12.34-12.43, Riga, Latvia, October 1992. 97.

[31] Desai, C., Zaman, M., Lightner, J., & Siriwardane, H. (1984). Thin-layer element for interfaces and joints. *International Journal for Numerical and Analytical Methods in Geomechanics, 8*(1), 19-43.

[32] Fakharian, K., & Evgin, E. (2000). Elasto-plastic modelling of stress-path-dependent behaviour of interfaces. *International Journal For Numerical And Analytical Methods In Geomechanics, 24*(2), 183-199.

[33] Tejchman, J., & Wu, W. (1995). Experimental and numerical study of sand–steel interfaces. *International Journal for Numerical and Analytical Methods in Geomechanics, 19*(8), 513-536.

[34] Hu, Liming, & Pu, Jialiu. (2004). Testing and modeling of soil-structure interface. *Journal of Geotechnical and Geoenvironmental Engineering, 130*(8), 851

[35] Desai, C., Drumm, E., & Zaman, M. (1985). Cyclic Testing and Modeling of Interfaces. *Journal of Geotechnical Engineering, 111*(6), 793-815.

[36] Moes, N., Dolbow, J., Belytschko, T. (1999) "A finite element method for crack growth without remeshing," *International Journal for Numerical Methods in Engineering*, 46, 131-150.

[37] Belytschko, T., Moes, N., Usui, S., Parimi, C. (2001) "Arbitrary discontinuities in finite elements," *International Journal for Numerical Methods in Engineering*, 50, 993-1013.

[38] Belytschko, T., Black, T. (1999) "Elastic crack growth in finite elements with minimal remeshing," *International Journal for Numerical Methods in Engineering*, 45, 601-620.

[39] Fleming, M., Chu, A., Moran, B., Belytschko, T. (1997) "Enriched element-free Galerkin methods for crack tip fields," *International Journal for Numerical Methods in Engineering*, 40, 1483-1504.

[40] Abaqus 6.14 Online Documentation

[41] Barenblatt, G. (1962). The Mathematical Theory of Equilibrium Cracks in Brittle Fracture. *Advances in Applied Mechanics,7*, 55-129.

[42] Miyakazi N, Ikeda T, Soda T, Munakata T (1993) Stress intensity factor analysis of interface crack using boundary element method— application of contour-integral method. Eng Frac Mech 45: 599–610

[43] Pathak, Himanshu, Singh, Akhilendra, & Singh, Indra. (2012). Numerical simulation of bi-material interfacial cracks using EFGM and XFEM. *International Journal of Mechanics and Materials in Design, 8*(1), 9-36.

[44] Gustafsson PJ, Hillerborg A. Improvements in concrete design achieved through the application of fracture mechanics. In: Shah SP, editor. Application of fracture mechanics to cementitious composites. Dordrecht, The Netherlands; 1985. p. 639‑80.

[45] Guinea GV, Planas J, Elices M. A general bilinear fit for the softening curve of concrete. Mater Struct 1994;27(2):99‑105.

[46] Reinhardt HW. Crack softening zone in plain concrete under static loading. Cem Concr Res 1985;15(1):42‑52.

[47] Comite Euro-International du Beton-Federation Internationale de la Precontrainte. CEB‑FIP Model Code. Lausanne: Switzerland; 1991.

[48] Bazant ZP, Becq-Giraudon E. Statistical prediction of fracture parameters of concrete and implications for choice of testing standard. Cem Concr Res 2001;32(4):529‑56.

[49] Rice, J R. (1978). Mechanics of quasi-static crack growth. United States. Retrieved from http://www.osti.gov/scitech/servlets/purl/6428286

[50] Stang, Henrik, & Aarre, Tine. (1992). Evaluation of crack width in FRC with conventional reinforcement. *Cement and Concrete Composites, 14*(2), 143-154.